Separable recruitment of DNA Polymerase α for initiation of DNA synthesis at replication origins and lagging-strand priming during replication elongation

Sarina Y. Porcella[1], Natasha C. Koussa, Colin P. Tang[1,2], Daphne N. Kramer[1], Priyanka Srivastava[1,3], Duncan J. Smith[1,4]

1. Department of Biology, New York University, New York, NY 10003, USA

2. Present address: Weill-Cornell Graduate School of Medical Sciences, New York, NY 10065, USA

3. Present address: School of Dentistry, UCSF Center for the Health Sciences, San Francisco, CA 94143

4. Corresponding author: duncan.smith@nyu.edu

Keywords: DNA replication, Lagging-strand synthesis, Replication origins, Checkpoint activation

Abstract

During eukaryotic DNA replication, DNA polymerase alpha/primase (Pol α) initiates synthesis on both the leading and lagging strands. It is unknown whether leading- and lagging-strand priming are mechanistically identical, and whether Pol α associates processively or distributively with the replisome. Here, we titrate cellular levels of Pol α in *S. cerevisiae* and analyze Okazaki fragments to study both replication initiation and ongoing lagging-strand synthesis *in vivo*. We observe that both Okazaki fragment initiation and the productive firing of replication origins are sensitive to Pol α abundance, but find that the absence of the replisome adaptor protein Ctf4 only impairs lagging-strand initiation. Our results suggest that distinct modes of Pol α recruitment exist for replication initiation and elongation, and are consistent with distributive association of Pol α with the replisome. Additionally, we observe that activation of the checkpoint becomes essential for viability upon severe depletion of Pol α, and demonstrate that this checkpoint requirement is due to impaired origin firing as opposed to reduced lagging-strand priming.

Author summary

Half of each eukaryotic genome is replicated continuously as the leading strand, while the other half is synthesized discontinuously as Okazaki fragments on the lagging strand. The bulk of DNA replication is completed by DNA polymerases ε and δ on the leading and lagging strand respectively, while synthesis on each strand is initiated by DNA polymerase α-primase (Pol α). Using the model eukaryote *S. cerevisiae*, we modulate cellular levels of Pol α and interrogate the impact of this perturbation on both replication initiation on DNA synthesis and cellular viability. We observe that Pol α associates dynamically at the replication fork for initiation on both strands. Although the initiation of both strands is widely thought to be mechanistically similar, we determine that Ctf4, a hub that connects proteins to the replication fork, specifically recruits Pol α to the lagging strand but is not required for leading-strand initiation. We also find that decreased leading-strand initiation results in a checkpoint response that is necessary for viability when Pol α is limiting. Because the DNA replication machinery is highly conserved from budding yeast to humans, this research provides insights into how DNA replication is accomplished throughout eukaryotes.

50 **Introduction**

51 DNA polymerase alpha/primase (Pol α) is responsible for initiating synthesis on the leading
52 strand and for each Okazaki fragment on the lagging strand (Kunkel and Burgers, 2008). The
53 ultimate contribution of Pol α to replication is limited, and bulk synthesis on the leading- and
54 lagging-strands is carried out by DNA polymerase epsilon (Pol ε) and polymerase delta (Pol δ),
55 respectively (Clausen et al., 2015; Daigaku et al., 2015; Pursell et al., 2007; Reijns et al., 2015).
56 Despite the fact that different DNA polymerases carry out the majority of DNA synthesis on the
57 two daughter strands, Pol α hands off synthesis predominantly to Pol δ during normal initiation
58 on both strands and during replication restart (Daigaku et al., 2015; Garbacz et al., 2018; Yeeles
59 et al., 2017; Miyabe et al., 2015). The use of the same initiating polymerase and downstream
60 partner implies a possible similarity between leading- and lagging-strand initiation. Indeed,
61 recent evidence from reconstituted replisomes suggests that leading-strand initiation can occur
62 via extension of the first Okazaki fragment synthesized on the lagging strand (Aria and Yeeles,
63 2018). However, analysis of repriming during damage bypass in the same reconstituted system
64 implies that leading- and lagging-strand repriming are mechanistically distinct (Taylor and
65 Yeeles, 2018).
66
67 Eukaryotic Okazaki fragments are considerably shorter than their prokaryotic
68 counterparts (Balakrishnan and Bambara, 2013; Ogawa and Okazaki, 1980). Okazaki fragment
69 length is quantized by the nucleosome repeat via interactions between nascent nucleosomes
70 and Pol δ in *S. cerevisiae* (Smith and Whitehouse, 2012) and *C. elegans* (Pourkarimi et al.,
71 2016). Okazaki fragment termini can also be positioned by nucleosomes in a reconstituted *S.*
72 *cerevisiae* replication reaction (Devbhandari et al., 2017). Both the distribution of Okazaki

73 fragment termini with respect to nucleosomes and the overall length profile of lagging-strand
74 products in *S. cerevisiae* and *C. elegans* are remarkably similar. Despite this apparent size
75 conservation, Okazaki fragment length can be altered on naked and non-chromatinized
76 templates *in vitro* by varying the concentration of Pol α (Kurat et al., 2017), analogous to the
77 impact of primase titration on lagging-strand synthesis in a reconstituted *E. coli* replication
78 system (Wu et al., 1992). Eukaryotic Okazaki fragment length can also be increased *in vivo* by
79 impairing nucleosome assembly (Smith and Whitehouse, 2012; Yadav and Whitehouse, 2016).
80
81 The maximum length of an Okazaki fragment is determined by the amount of single-stranded
82 DNA unwound at the replication fork before lagging-strand priming and extension. Thus, longer
83 fragments would result in the exposure of long stretches of damage-prone single-stranded DNA.
84 Shorter Okazaki fragments would expose shorter stretches of ssDNA, but at the likely cost of
85 increasing the contribution of the error-prone Pol α to synthesis of the lagging daughter strand
86 (Kunkel, 2011; Reijns et al., 2015). However, it is currently unclear to what extent changing
87 Okazaki fragment length directly impacts cellular fitness. Reduced DNA polymerase activity
88 upon aphidicolin treatment induces chromosome breakage and genomic rearrangements at
89 fragile sites in mammals (Glover et al., 1984). Analogously, reducing the intracellular
90 concentration of Pol α in *S. cerevisiae* increases S-phase duration, sensitivity to DNA damaging
91 agents, and chromosomal rearrangements at defined sites (Lemoine et al., 2005; Song et al.,
92 2014). The detrimental effects of Pol α depletion on genome integrity could arise due to
93 defective leading- or lagging-strand initiation, both of which are dependent on Pol α.
94
95 Ctf4 was originally identified as a chromosome transmission fidelity mutant (Kouprina et al.,
96 1992). Subsequent studies have identified multiple roles for Ctf4 in DNA metabolism. Ctf4 is not

97 only required for the establishment of sister chromatin cohesion (Borges et al., 2013; Hanna et
98 al., 2001), but also links Pol α to the replication fork via interaction with the replicative helicase
99 (Gambus et al., 2009; Tanaka et al., 2009), and is required for error-free lesion bypass
100 (Fumasoni et al., 2015) and rDNA maintenance (Villa et al., 2016). At least some of these roles
101 for Ctf4 are independent of Pol α binding. The metazoan Ctf4 ortholog, AND-1 also stimulates
102 Pol α binding to chromatin, and is required for efficient DNA replication (Zhu et al., 2007).
103 Interestingly, despite the conserved contribution of Ctf4 to Pol α recruitment, *ctf4Δ S. cerevisiae*
104 strains have been demonstrated to synthesize identically sized Okazaki fragments to wild-type
105 cells (Borges et al., 2013). Additionally, the Ctf4 protein has a minimal effect on the priming of
106 either DNA strand in reconstituted replication reactions (Kurat et al., 2017). Thus, the
107 contributions of Ctf4 to Pol α recruitment for origin firing and Okazaki fragment initiation have
108 not been fully elucidated *in vivo*.
109
110 Here, we analyze Okazaki fragments to directly test the effects of Pol α depletion on origin firing
111 efficiency and Okazaki fragment initiation in *S. cerevisiae*. We find that Pol α is recruited
112 distributively to the replication fork for priming on both strands, but that only lagging-strand
113 priming is dependent on Ctf4. Impaired Okazaki fragment priming is well tolerated, but reduced
114 origin firing leads to a strict dependence on checkpoint activation for continued viability.
115
116 **Results**
117
118 **Cells with reduced levels of Pol α synthesize longer Okazaki fragments *in vivo.***
119

120 To investigate the effect of Pol1 depletion on leading- and lagging-strand priming during
121 replication, we modified the approach of Petes and co-workers (Lemoine et al., 2005; Song et
122 al., 2014), limiting expression of *POL1* by replacing its promoter with *pGAL1*. Expression of Pol1
123 from galactose-inducible promoters generates a stable polypeptide that can persist for several
124 cell cycles (Muzi Falconi et al., 1993). Therefore, to facilitate turnover of pre-existing Pol1 and
125 focus on the acute effects of depletion, we additionally fused an N-terminal degron to the *POL1*
126 coding sequence. Western-blot analysis indicated that the concentration of this GAL1-
127 expressed, degron-tagged Pol1 (GDPol1) could be specifically and rapidly modulated within 4h
128 (Fig. 1A). The lower band marked with an asterisk in GDPol1-myc Western blots is a
129 degradation product resulting from degron-tagging (see Fig. S1A). All cultures were grown in
130 media supplemented with 3% raffinose to avoid indirect effects due to carbon limitation. Pol1
131 levels oscillate through the cell cycle when the protein is endogenously expressed, but not when
132 expression is driven by galactose (Muzi Falconi et al., 1993). Because Pol1 concentration is not
133 constant even within S-phase (Muzi Falconi et al., 1993), and only 2/3 of cells in an
134 asynchronous population are in G1, G2 or M phase, we compared wild-type POL1 expression
135 during S phase to 0.5% and 0.05% galactose in our inducible system at the zero and 60 minute
136 timepoints after release from alpha-factor-mediated G1 arrest (Fig. S1A). We estimate that the
137 expression level at 0.05% galactose is slightly lower than endogenous during the relevant phase
138 of the cell cycle, consistent with several phenotypes described below.
139
140 To analyze Okazaki fragment biogenesis, we crossed the *GDPOL1* allele into a strain
141 background in which DNA ligase I (Cdc9) can be depleted from the nucleus by rapamycin
142 treatment using the anchor away method (Haruki et al., 2008). Nuclear depletion of Cdc9
143 enriches nucleosome-sized Okazaki fragments (Fig. S1B), similarly to transcriptional repression

144 of Cdc9 (Smith and Whitehouse, 2012; Yadav and Whitehouse, 2016). Robust detection of
145 Okazaki fragments was possible after 1h rapamycin treatment: therefore, all Okazaki fragment
146 labeling and sequencing experiments were conducted after a 4h sugar switch to reduce Pol α
147 levels, followed by 1h ligase depletion by rapamycin (Fig. 1B).
148
149 By end-labeling unligated Okazaki fragments, we observed that cells with wild-type *POL1* did
150 not show an increase in Okazaki fragment length under low-galactose growth conditions (Fig.
151 1C). This result was highly reproducible (another representative gel is shown in Fig. S1C). By
152 contrast, in the *GDPOL1* strain Okazaki fragment length was normal at Pol1 concentrations
153 down to a critical concentration corresponding to growth in 0.014% galactose (Fig. 1D,
154 representative replicate experiments are shown in Fig. S1D-E). At 0.014% galactose the
155 Okazaki fragment length profile was shifted slightly upwards such that fragments were clearly
156 still phased by nucleosomes, while lower galactose concentrations (0.005%) showed a
157 significant loss of signal (Fig. 1D cf. lanes 5&6). To confirm that this loss of signal reflected a
158 further length increase (and therefore a reduction in the number of ends being labeled), we
159 analyzed Okazaki fragments by Southern blot using a whole-genome probe: as anticipated for
160 severely perturbed lagging-strand priming, Okazaki fragments at 0.005% galactose were
161 significantly larger than at 0.014% (Fig. 1E). We conclude that limiting levels of Pol α lead to
162 reduced priming frequency on the lagging strand, resulting in longer Okazaki fragments, and
163 that *S. cerevisiae* cells can sustain growth when Okazaki fragment length is substantially
164 increased. These data are consistent with the presence of multiple Pol α complexes at the
165 replication fork and/or the repeated, distributive recruitment of Pol α to the replisome for lagging-
166 strand priming during replication, since the priming kinetics of a single Pol α complex stably
167 associated with the replisome would be unaffected by cellular Pol α concentrations (see
168 discussion).

169

170 To analyze the location of Okazaki fragment termini, we purified and sequenced Okazaki
171 fragments (Smith and Whitehouse, 2012) from wild-type and *GDPOL1* strains shifted to low
172 galactose concentrations for 4h before 1h ligase depletion. Galactose concentration does not
173 significantly affect the distribution of Okazaki fragment termini in wild-type cells (Fig. 1F).
174 However, we observed that both the 5' (Fig. 1G) and 3' (Fig. S1F) termini of Okazaki fragments
175 in *GDPOL1* cells were less enriched at nucleosome dyads during growth in 0.005% galactose
176 (Fig. 1G); an intermediate effect is observed at 0.014% galactose. Pol1 interacts with the FACT
177 component Spt16 (Foltman et al., 2013): furthermore, Pol α contains a histone-binding motif for
178 H2A and H2B and it is implicated in the maintenance of repressive chromatin during replication
179 (Evrin et al., 2018). The change in the distribution of Okazaki fragment ends upon severe Pol α
180 depletion could plausibly arise due to defects in chromatin assembly under conditions of low Pol
181 α as observed in histone chaperone mutants (Smith and Whitehouse, 2012; Yadav and
182 Whitehouse, 2016). An alternative, though not mutually exclusive, possibility is that Okazaki
183 fragment processing is impaired when priming frequency is reduced.
184

185 **Reduced levels of Pol α lead to a global decrease in replication origin firing efficiency**

186

187 Replication origin firing efficiency can be quantitatively inferred from the distribution of Watson-
188 and Crick-strand Okazaki fragments after deep sequencing (McGuffee et al., 2013; Petryk et al.,
189 2016; Pourkarimi et al., 2016). By comparing the fraction of Okazaki fragments mapping to the
190 Watson and Crick strands in the region ±10 kb from the replication origin midpoint, an Origin
191 Efficiency Metric (OEM) can be calculated (McGuffee et al., 2013). Okazaki fragment
192 distributions on the right arm of chromosome 10 are shown in Fig. 2A, and genome-wide origin

193 efficiencies are quantified as OEM in Fig. 2B. Comparisons between replicate datasets were
194 most robust at high Pol α levels. We observed more variability in origin efficiency across
195 replicates at lower Pol α levels (Fig. S2A), although each Pol α concentration maintains a
196 consistent trend across replicates (Fig. S2B). Data in Fig. 2 represent the mean origin efficiency
197 across three replicate experiments. While origin efficiency was unaffected by galactose
198 concentration in wild-type cells, average firing efficiency was linearly reduced in the *GDPOL1*
199 strain at progressively lower galactose concentrations (Fig. 2B).
200
201 Interestingly, we observed that the efficiency of productive replication origin firing is impaired at
202 similar Pol1 concentrations (0.023% galactose) to those that impair Okazaki fragment initiation
203 (0.014% galactose) (Fig 1D&E). This dramatic decrease in origin efficiency likely contributes to
204 the slow growth (Fig. S3A), cell-cycle delay (Fig. S3B & (Lemoine et al., 2005)), and
205 accumulation of S-phase cells (Fig. S3C) observed under limiting Pol1 conditions. Even at low
206 Pol1 concentrations, we observe no change in fork arrest at tDNAs (Fig. S4) – the major sites of
207 replisome stalling in the *S. cerevisiae* genome (Ivessa et al., 2003; Osmundson et al., 2017).
208 Thus, we conclude that the global changes in the direction of replication-fork movement upon
209 Pol1 depletion most likely stem from changes in origin efficiency as opposed to widespread
210 differences in replication-fork stalling or arrest.
211
212 If one or more Pol α complexes is stably recruited to and maintained in the replisome upon
213 leading-strand initiation, reducing Pol α to sub-stoichiometric levels would privilege early and/or
214 efficient replication origins while disproportionately reducing the efficiency of late and/or
215 inefficient origins. By contrast, distributive recruitment would lead to reduced efficiency of all
216 origins under limiting Pol α conditions. We analyzed origin efficiency in the *GDPOL1* strain as a

217 function of normal firing efficiency. As the concentration of Pol α was decreased, firing of all
218 origins became less efficient regardless of their normal efficiency (Fig. 2C & S2C). Further
219 analysis indicated that the activity of each origin is reduced in proportion to its original firing
220 efficiency (Fig. 2D). Both early- and late-firing replication origins showed a global decrease in
221 firing efficiency at low Pol1 concentrations (Fig. 2E).
222
223 **Ctf4 stimulates Pol α recruitment for Okazaki fragment initiation but not productive origin**
224 **firing**
225
226 Ctf4 has previously been shown to stimulate the recruitment or maintenance of Pol α and
227 several additional proteins to the replisome (Gambus et al., 2009; Samora et al., 2016; Tanaka et
228 al., 2009; Villa et al., 2016). Indeed, it has been proposed that a Ctf4 homotrimer could
229 simultaneously recruit two Pol α complexes while the third subunit is tethered to the replisome
230 via interaction with the Sld5 component of the Cdc45/MCM2-7/GINS (CMG) complex (Simon et
231 al., 2014). *CTF4* is nonessential in *S. cerevisiae*; the absence of Ctf4 does not affect lagging-
232 strand synthesis in a reconstituted *S. cerevisiae* replication system (Kurat et al., 2017), and
233 Okazaki fragment length is unchanged in otherwise wild-type *ctf4Δ* cells (Borges et al., 2013).
234 Pol1 contains a Ctf4 interacting peptide (CIP) motif that is necessary for Ctf4 to recruit Pol α to
235 the fork: mutating specific residues in the CIP abolishes the interaction between Pol1 and Ctf4
236 without affecting the recruitment of other proteins to the fork (Simon et al., 2014, Villa et al.,
237 2016). To investigate the effect of Ctf4 on leading- and lagging-strand synthesis under limiting
238 Pol α conditions, we abrogated the Pol α-Ctf4 interaction via deletion of *CTF4* or mutation of the
239 Pol1 CIP box (*pol1-4A*) (Simon et al., 2014). We analyzed Okazaki fragments from these strains
240 using, end labeling, Southern blots, and sequencing.

241

242 In the absence of Ctf4, Okazaki fragments increase in length at ~0.06% galactose (Fig. 3A,)–
243 significantly higher than the 0.014% observed for a *CTF4* wild-type strain (cf. Fig. 1D&E). The
244 *GDpol1-4A* strain showed a similar increase in Okazaki fragment length to the *ctf4Δ* strain, with
245 longer fragments observed at 0.05% galactose (Fig. 3B&C, replicate experiments in Fig.
246 S5A&C). These longer Okazaki fragments at sub-endogenous Pol1 levels (0.05%) were further
247 confirmed by Southern blot with a whole genome probe (Fig. S5B). Continued growth while
248 synthesizing long Okazaki fragments was observed down to 0.005% galactose (Fig. 3B&C),
249 with a significant reduction in viability observed only at the lowest concentration tested (0.005%;
250 Fig. S5D). It has previously been demonstrated that overall cellular levels of Pol1 are unaffected
251 by the absence of, or a failure to bind, Ctf4 (Villa et al., 2016). Our data therefore suggest that
252 Ctf4 helps to maintain robust lagging-strand priming when Pol α activity is reduced, although
253 cellular levels of Pol α are sufficient for normal Okazaki fragment initiation even in its absence
254 (Fig. 3A and (Borges et al., 2013)).

255

256 We analyzed replication origin firing efficiency in the absence of Ctf4-Pol α interactions by
257 sequencing Okazaki fragments from *ctf4Δ;GDPOL1* and *GDpol1-4A s*trains grown at various
258 galactose concentrations (Fig. 3C). Data shown are the average of two replicates. Correlations
259 between replicates were extremely robust at all concentrations of Pol α (Fig. S6A&B). In the
260 absence of Ctf4, cells maintained normal levels of origin firing down to 0.032% galactose, after
261 which a linear decrease in firing efficiency was apparent (Fig. 3D). The *GDpol1-4A* strain
262 showed normal origin efficiency down to 0.023% galactose, followed by a decrease at 0.014% a
263 further reduction at 0.005% galactose (Fig. 3E). Because origin firing efficiency at low Pol α is
264 either unaffected or very slightly increased by the absence of Ctf4-Pol α interaction (cf. Fig. 2B

265 and 3D&E), while intermediate levels of Pol α support normal levels of origin firing under
266 conditions where Okazaki fragment length is increased (Fig. 3A-C), we conclude that Ctf4 does
267 not stimulate replication-origin firing even at low concentrations of Pol α.
268
269 Each rDNA repeat in *S. cerevisiae* contains a replication origin. rDNA size has been reported to
270 change due to deletion of *CTF4* (Sasaki and Kobayashi, 2017) or lithium acetate transformation
271 (Kwan et al., 2016). Expansion of the rDNA repeat increases the total number of origins in the
272 genome, and could thereby depress origin firing elsewhere (Shyian et al., 2016; Yoshida et al.,
273 2014). We investigated whether the origin efficiency in *ctf4Δ* cells is impacted by the size of the
274 rDNA array. The proportion of Okazaki fragments mapping to the rDNA in *ctf4Δ* libraries was
275 around 70% higher than in *CTF4* or *pol1-4A* libraries (Fig. S5E), consistent with substantial
276 array expansion in the absence of Ctf4 (Sasaki and Kobayashi, 2017). However, this change in
277 rDNA copy number appears to have a minimal effect on genome-wide origin firing efficiency.
278
279 To address the possibility that chromatin assembly defects may be the sole cause of longer
280 Okazaki fragments upon Pol α depletion, we analyzed the distribution of Okazaki fragment
281 termini around nucleosome dyads at 0.05% galactose – a concentration that generates longer
282 Okazaki fragments only in the context of the *ctf4Δ;GDPOL1* and *GDpol1-4A s*trains (Fig. 3A-C)
283 but not the wild-type strain (Fig. 1C). At this intermediate Pol α concentration, the distribution of
284 Okazaki fragment 5' and 3' termini was highly nucleosome-biased and very similar between
285 wild-type, *GDPOL1, ctf4Δ;GDPOL1,* and *GDpol1-4A s*trains (Fig. 3F & S5F-G). At low Pol α
286 concentrations, the distribution of Okazaki fragment 5' and 3' termini lost nucleosome patterning
287 in *ctf4Δ;GDPOL1,* and *GDpol1-4A* (Fig. S5F-G), similarly to the behavior of the wild-type
288 *GDPOL1* strain (Fig. 1G). However, the alignment of Okazaki fragment 5' or 3' end locations
289 with nucleosome dyads was lost at higher Pol α concentrations in *ctf4Δ;GDPOL1* strains

290 compared to *GDpol1-4A* (Fig. S5F-G), consistent with an additional contribution of Ctf4 to
291 chromatin assembly beyond Pol α recruitment.
292
293 *ctf4Δ;GDPOL1,* and *GDpol1-4A* cells grown at 0.05% galactose show increased Okazaki
294 fragment length (Fig. 3B-C) but no defect in the nucleosome patterning of Okazaki fragment
295 termini (Fig. 3F). Therefore, Okazaki fragment length can be increased by reduced Okazaki
296 fragment initiation in the absence of an accompanying chromatin assembly defect. We note that
297 these data are not inconsistent with impaired nucleosome assembly at severely reduced Pol α
298 concentrations contributing to a further increase in Okazaki fragment length. We conclude that
299 Ctf4-mediated recruitment of Pol α to the replisome does not stimulate replication-origin firing in
300 *S. cerevisiae*, but plays an important role in maintaining the robustness of lagging-strand
301 priming to fluctuations in the availability of Pol α.
302
303 **Checkpoint activation is required for viability when origin firing is reduced, but not when**
304 **lagging-strand priming is perturbed**
305
306 In response to DNA damage or replication stress, a checkpoint signaling cascade is initiated
307 and culminates in the phosphorylation of the effector kinase Rad53 (Ciccia and Elledge, 2010).
308 We analyzed Rad53 phosphorylation in the *GDPOL1* strain after a switch to low galactose.
309 Substantial phosphorylation of Rad53 was observed only at concentrations below 0.023%
310 galactose (Fig. 4A) – a concentration at which both origin firing and Okazaki fragment initiation
311 are perturbed (Figs. 1&2). To further investigate the interplay between Pol α depletion,
312 increased Okazaki fragment length, decreased origin firing, and checkpoint activation, we
313 combined the *GDPOL1* allele with deletion of *MEC1* (with additional deletion of *SML1* to
314 maintain viability of *mec1Δ* cells). Growth of the *GDPOL1; mec1Δ; sml1Δ* mutant was impaired

315 at 0.05% galactose and virtually absent at 0.014% and 0.005% galactose (Fig. 4B). Thus,
316 checkpoint-deficient cells apparently cannot survive with limiting Pol α. Consistent with a rapid
317 loss of viability upon Pol1 depletion in checkpoint-deficient cells, we were unable to robustly
318 detect long Okazaki fragments in *GDPOL1; mec1Δ; sml1Δ* cells shifted to low concentrations of
319 galactose (Fig. 4C). Okazaki fragment length was normal in this strain at galactose
320 concentrations above 0.023%.
321
322 To test the contributions of the DNA damage checkpoint (DDC), mediated by Rad9, and the
323 DNA replication checkpoint (DRC), mediated by Mrc1, to survival under limiting Pol α
324 conditions, we analyzed the growth of *GDPOL1* strains in combination with *rad9Δ*, *mrc1Δ*, or
325 the non-phosphorylatable *mrc1*^{AQ} allele (Osborn and Elledge, 2003) (Fig. 4B&D; the full range of
326 galactose concentrations is shown in Fig. S7A-B). *GDPOL1* cells showed robust growth at low
327 Pol1 concentrations in both *rad9Δ* and *mrc1Δ* strain backgrounds. *GDPOL1;mrc1*^{AQ}*; rad9Δ*
328 cells did not grow at 0.005% galactose (Fig. 4D), confirming that the inviability of *GDPOL1;*
329 *mec1Δ; sml1Δ* cells under these conditions is due to the absence of functional DDC and DRC
330 signaling. We note that *GDPOL1;mrc1*^{AQ} cells grow as well as *GDPOL1* cells at all
331 concentrations tested; this suggests that the slight growth defect at 0.005% galactose observed
332 in *GDPOL1;mrc1Δ* cells is most likely due to decreased replication fork speed (Szyjka et al.,
333 2005; Yeeles et al., 2017) in combination with decreased origin firing (Fig. 2B) as opposed to
334 impaired DRC activity. In summary, checkpoint activation is required for viability under
335 conditions of severe Pol α depletion: this activation can proceed via either the DDC or the DRC.
336
337 We investigated the sensitivity of *GDPOL1* cells during Pol α depletion to either replication
338 stress or DNA damage by testing growth defects in the presence of 1 mM hydroxyurea or
339 0.008% methyl methanesulfonate (Fig. S7A-D). We observed that growth defects in the

340 presence of HU or MMS were exacerbated by lowering the concentration of Pol α; this effect
341 was apparent in both checkpoint-proficient and checkpoint-deficient strains. Indeed, in the
342 presence of 1 mM HU a significant growth defect can be observed at 0.05% galactose – a
343 concentration at which neither origin firing nor lagging-strand priming is impaired in strains
344 proficient for Ctf4-Pol α interaction.
345
346 To determine whether the requirement for checkpoint activation was due to deregulated lagging-
347 strand priming or impaired leading-strand initiation, we compared the growth of
348 *GDPOL1;mec1Δ;sml1Δ* strains with and without *CTF4* or *pol1-4A* at 0.5% and 0.05% galactose.
349 Loss of Ctf4-Pol α interactions affects Okazaki fragment initiation at relatively high Pol α
350 concentrations, before leading-strand initiation is impaired. Thus, *ctf4Δ* and *pol1-4A* are
351 effectively separation of function mutants: at 0.05% galactose, Okazaki fragment initiation is
352 reduced by the absence of Ctf4-mediated recruitment of Pol α while leading-strand initiation is
353 not (Fig. 3). *GDPOL1;mec1Δ;sml1Δ;ctf4Δ* cells grow slowly relative to *MEC1* or *CTF4* cells:
354 however, growth was minimally affected by galactose concentrations (Fig. 4E). This result is
355 recapitulated with *GDpol1-4A;mec1Δ;sml1Δ* strain, which showed essentially no growth defect
356 at either Pol α concentration (Fig. 4E). Therefore, perturbed lagging-strand synthesis does not
357 directly cause growth defects the absence of a functional checkpoint. We conclude that cells
358 with limiting Pol α become reliant on the checkpoint predominantly due to decreased replication
359 origin firing as opposed to increased Okazaki fragment length.
360
361 **Discussion**
362
363 **Cellular impact of perturbed leading- and lagging-strand initiation.**
364

365 Checkpoint activation is required for robust DNA synthesis, and therefore for viability, when
366 origin firing is significantly reduced (Fig. 4). This observation is consistent with genetic
367 interactions in *S. cerevisiae* – for example similar negative genetic interactions of *rad9Δ* with
368 alleles of the catalytic subunits of each of the three replicative polymerases (Dubarry et al., 2015). It will be interesting to determine the contributions of leading- and lagging-strand
369
370 perturbations to the many reported phenotypes resulting from *pol1* mutation or Pol1 depletion –
371 for example increased trinucleotide repeat expansion rate and size (Shah et al., 2012), and
372 increased chromosome fragility (Lemoine et al., 2005; Song et al., 2014). Furthermore,
373 mutations that reduce the levels of functional Pol α (Van Esch et al., 2019) or Pol ε (Bellelli et al., 2018) in mammalian cells increase replication stress linked to reduced origin firing, highlighting
374
375 the relevance of these studies beyond budding yeast.
376
377 **Pol α initiation on the leading and lagging strands**
378
379 Our data indicate that both origin firing and Okazaki fragment initiation in *S. cerevisiae* are
380 robust with respect to fluctuations in Pol α availability. Pol α concentration does not normally
381 limit primer synthesis and/or utilization, and significant disruption of Okazaki fragment synthesis
382 or replication initiation is only observed at very low Pol α concentrations (Fig. 1). Because cells
383 with limiting Pol α synthesize longer Okazaki fragments, as opposed to fewer Okazaki
384 fragments of normal size, our data suggest that Pol α acts distributively *in vivo* as opposed to
385 being stably tethered at the replication fork. We additionally note that the increase in Okazaki
386 fragment length upon Pol α depletion is consistent with a priming mechanism in which there is
387 no strict coupling between DNA unwinding and primer synthesis *in vivo*.
388

389 Although the Ctf4 protein has little to no effect on lagging-strand synthesis in chromatinized
390 reconstituted systems (Kurat et al., 2017), we observe that Ctf4 stimulates lagging-strand
391 priming *in vivo*. In the absence of Ctf4, Okazaki fragment length can still be modulated by Pol α
392 concentration (Fig. 3). Thus, in light of the distributive action of Pol α, a simple model is that Ctf4
393 acts by increasing the local concentration of Pol α at the elongating replication fork. An
394 alternative possibility is that Ctf4 maintains two copies of Pol α at each replisome under normal
395 conditions. It is unclear what underlies the differential Ctf4-sensitivity of reconstituted and *in vivo*
396 lagging-strand synthesis. Our data also show that, unlike ongoing Okazaki fragment priming
397 during lagging-strand synthesis, the productive initiation of DNA synthesis at replication origins
398 is independent of Ctf4 *in vivo* (Figs. 2&3). A recent report demonstrated that leading-strand
399 initiation can occur via extension of the first Okazaki fragment from the opposite replication fork,
400 and that the two replisomes are inter-dependent during this establishment phase (Aria and
401 Yeeles, 2018). The close proximity of the two replisomes at this stage could underlie the Ctf4-
402 independence of replication-origin firing.
403
404 All replication origins are affected by Pol α depletion, in proportion to their normal firing
405 efficiency and without dependence on their normal firing time or efficiency (Fig. 2D). Therefore,
406 it is unlikely that the reduction in origin firing is a direct result of checkpoint activation. Our data
407 suggest that the origin firing program is determined by the relative accessibility of licensed
408 origins to limiting soluble firing factors, even when overall origin firing is reduced. Spatial
409 clustering of replication origins, mediated by Fkh transcription factors in *S. cerevisiae*, likely
410 plays a significant role in this accessibility (Knott et al., 2012). We note that coordinately down-
411 regulating the efficiency of all origins, as opposed to selectively reducing the efficiency of a
412 subset, represents a robust strategy to maintain the evolutionarily selected co-orientation of

413 deleterious transcription events with replication (Chen et al., 2019; Hamperl et al., 2017;
414 Osmundson et al., 2017; Tran et al., 2017).
415
416 **Chromatin and lagging-strand synthesis**
417
418 Pol α acts distributively on naked DNA in reconstituted replication reactions (Yeeles et al., 2017).
419 Chromatin reduces Okazaki fragment size *in vitro,* and has therefore been proposed to make
420 Pol α more processive (Kurat et al., 2017). Our data suggest that Pol α acts distributively on
421 chromatin *in vivo*, but is present at saturating concentrations that would minimize the difference
422 between distributive or processive activity. Our data do, however, support an intimate interaction
423 between chromatin and lagging-strand priming. Extreme depletion of Pol α leads to Okazaki
424 fragment distributions consistent with impaired chromatin assembly (Fig. 1G and S5F-G). Since
425 Ctf4 connects Pol α to the replicative helicase, its absence also impacts chromatin dynamics
426 during DNA replication (Evrin et al., 2018). However, perturbed Okazaki fragment initiation in the
427 absence of Ctf4-mediated recruitment of Pol α to the fork can generate longer Okazaki
428 fragments in the absence of an obvious chromatin assembly defect (Fig. 3F). It is also possible
429 that the increased length of Okazaki fragments reported in histone chaperone mutants (Smith
430 and Whitehouse, 2012; Yadav and Whitehouse, 2016) represents an underlying defect in
431 priming.
432
433

434 **MATERIALS AND METHODS**

435 **Yeast strains**

436 All yeast strains were W303 *RAD5+*, and contained additional mutations required for anchor-
437 away depletion of Cdc9. The genotype of the wild-type strain is *mata, tor1-1::HIS3,*
438 *fpr1::NatMX4, RPL13A-2xFKBP12::TRP1, CDC9-FRB::HygMX*. The *pol1-4A* mutant from
439 (Simon et al., 2014) was generated using the CRISPR/Cas9 system in *S. cerevisiae* as
440 previously described (Dicarlo et al., 2013). Briefly, a guide RNA was synthesized specific to the
441 CIP box in *POL1* that could not be cleaved if repaired with donor sequence with D141A, D142A,
442 L144A and F147A mutations and 100 bp of homology on both sides. This created a markerless
443 strain that was confirmed through Sanger sequencing. After transformations, strains were grown
444 on YPD to lose the Cas9 and gRNA plasmids. Additional gene deletions, and replacement of
445 the *POL1* promoter, were carried out by PCR-mediated replacement in a wild-type strain, and
446 introduced into the desired background by cross.

447

448 **Cell growth, cell-cycle synchronization, and spot tests**

449 All strains were grown at 30°C, starting in YEP with 0.5% galactose plus 3% raffinose, unless
450 otherwise noted. To deplete Pol1 levels, cultures were sugar switched by growing overnight to
451 log phase then washing the cells with sterile deionized water then sterile YEP before being
452 inoculated into fresh YEP media with various galactose concentrations supplemented with 3%
453 raffinose.

454

455 For short-term experiments, strains were grown for four hours after the sugar switch before
456 adding rapamycin for one hour of ligase repression. Cells were collected four hours after the
457 sugar switch for western blot analysis.

458 For cell-cycle synchronization, cultures were sugar-switched at log phase and then added
459 5g/mL alpha factor to synchronize cells in G1 phase. Cells were released into S phase and were
460 collected every 15 minutes by centrifugation at 4°C then stored at -80°C or by immediately fixing
461 cells in 70% ethanol.
462 For spot tests, yeast cells were washed then counted. Similar numbers of cells were plated onto
463 various galactose concentrations with or without 2mM hydroxyurea (Sigma H8627) or 0.008%
464 methyl methanesulfonate (Sigma 129925) at a 1:5 dilution series and grown overnight for two
465 days at 30°C unless indicated otherwise.
466
467 **Fluorescence-activated cell sorter (FACS) analysis**
468 Cells were collected after release from G1 arrest every 15 minutes and fixed in 70% ethanol and
469 incubated at 4°C overnight. Fixed cells were then spun down and resuspended in 50mM sodium
470 citrate with RNase A (Fisher 50-153-8126) for 1 hour at 50°C. Next, with the addition of
471 proteinase K (MP Biomedicals) the samples were incubated for 1 hour at 50°C. Cells were then
472 stained with SYTOX green (Fisher S7020) then sonicated and processed using a Becton
473 Dickinson Accuri.
474
475 **Western blotting**
476 Samples were collected by centrifugation and washed with deionized water and stored at -80°C
477 before lysate preparation. Lysates were prepared by five-minute resuspension in 600uL 2M
478 lithium acetate on ice, pelleted, resuspended in 600uL 400mM sodium hydroxide at room
479 temperature for five minutes, pelleted, and resuspended in Laemmli buffer with 5% beta-
480 mercaptoethanol prior to boiling, then briefly pelleted immediately prior to loading the lysate onto
481 a SDS-PAGE gel. Samples were transferred to PVDF, blocked with 5% milk and probed with C-
482 Myc antibody (Genscript A00173-100), Rad53 antibody (Abcam ab104232), histone H4
483 antibody (Abcam ab10158), or actin antibody (Thermofisher Scientific MA1-744).

484

485 **Okazaki fragment analysis by gel electrophoresis**

486 Following the sugar switch methods above, Okazaki fragments were accumulated by adding
487 rapamycin (Spectrum 41810000-2) to 1ug/mL to anchor away Cdc9, which is tagging with FRB,
488 for 1h (Haruki et al., 2008). These cells were collected through centrifugation and immediately
489 processed or stored at -80°C. Genomic preps from spheroplasts were completed as previously
490 described (Smith and Whitehouse, 2012). For end-labeling, 5uL of genomic DNA was labeled
491 using a 50uL reaction with 5U Klenow exo- (NEB M0212L) and α-dCTP (Perkin Elmer
492 BLU513H500UC) at a final concentration of 33 nM. Reactions were then ethanol precipitated to
493 remove excess label. Normalized amounts (from either native gel or previous experiment) were
494 loaded onto a 1.3% denaturing agarose gel. After electrophoresis, gels were then blotted onto
495 nitrocellulose membrane (Fisher 45-000-932) overnight. Membranes were then dried and
496 exposed to phosphor screens.
497 For southern blot analysis, unlabeled genomic DNA was normalized to total genomic DNA, and
498 run on 1.3% denaturing agarose gels. After electrophoresis, the gel was blotted onto a
499 nitrocellulose membrane (Fisher 45-000-932) overnight. Next the membrane was crosslinked
500 and washed, then hybridized overnight with a probe synthesized with random hexamers labeling
501 kit (Fisher 18187-013) and sheared genomic DNA. After two low stringency washes,
502 membranes were dried then exposed to phosphor screens.

503

504 **Okazaki fragment purification, sequencing, and analysis**

505 Genomic DNA was boiled at 95°C for 5 min then salt was added to 300mM NaCl, pH 12.
506 Purification of Okazaki fragments was accomplished by running the denatured genomic DNA
507 through 400 ul Source 15Q (VWR 89128-854), binding at 300 mM NaCl, pH 12. DNA was

508 eluted in 50mM steps until 900mM NaCl, pH 12, fractions kept were 800mM, 850mM, and
509 900mM, these were stored at -20°C. DNA was ethanol precipitated then treated with RNase
510 cocktail (Thermo Fisher AM2286) for 1h at 37°C to remove any RNA. Next, these reactions
511 were ethanol precipitated then run through Illustra microspin G-50 columns (Fisher 27-5330-02).
512 The single-strand Okazaki fragments were boiled at 95°C for 5 min and cooled quickly on ice
513 and up to 1ug of purified fragments were ligated with T4 DNA ligase (Fisher 50305904) to 1ug
514 of adaptors with single-stranded overhangs that were generated as previously described (Smith
515 and Whitehouse, 2012). Purified libraries were amplified (12-16 cycles) using Illumina Truseq
516 primers according to Illumina protocols, but with Phusion (NEB M0530L). Paired-end
517 sequencing (2 × 75 bp) was carried out on an Illumina Next-seq 500 platform. FASTQ files were
518 aligned to the s288c reference genome using the Bowtie (v2.3.2). The files were converted,
519 then bad quality reads and PCR duplicates were removed using the Samtools suite (v1.9). Then
520 the genomic coverage was calculated using the Bedtools suite (v2.27.1) in a strand-specific
521 manner to make stranded bed files. Origin efficiency metric analysis was achieved through
522 calculating the strand bias in 10kb windows around predefined origins as previously described
523 (McGuffee et al., 2013) with the origin list from the same source. To map the Okazaki fragments
524 ends relative to known nucleosome dyads (Jiang and Pugh, 2009), 5' and 3' fragment ends were
525 extracted from previously generated bed files and a meta-analysis was completed as previously
526 described (Smith and Whitehouse, 2012).
527

528 **ACKNOWLEDGEMENTS**

529 We thank the NYU Gencore for assistance, and members of the Smith lab for helpful discussions.
530 Supported by grants from the NIH (R01GM114340) and the Searle Scholars Program to D.J.S

531 **REFERENCES**

532 Aria, V., and Yeeles, J. T. P. (2018). Mechanism of Bidirectional Leading-Strand Synthesis
533 Establishment at Eukaryotic DNA Replication Origins. Mol Cell

534 Balakrishnan, L., and Bambara, R. A. (2013). Okazaki fragment metabolism. Cold Spring Harb
535 Perspect Biol *5*,; doi: 10.1101/cshperspect.a010173.

536 Bellelli, R., Borel, V., Logan, C., Svendsen, J., Cox, D. E., Nye, E., Metcalfe, K., O'Connell, S.
537 M., Stamp, G., Flynn, H. R., Snijders, A. P., Lassailly, F., Jackson, A., and Boulton, S. J.
538 (2018). Polε Instability Drives Replication Stress, Abnormal Development, and
539 Tumorigenesis. Mol Cell *https://doi.org/10.1016/j.molcel.2018.04.008,*

540 Borges, V., Smith, D. J., Whitehouse, I., and Uhlmann, F. (2013). An Eco1-independent sister
541 chromatid cohesion establishment pathway in S. cerevisiae. Chromosoma *122*, 121-134.

542 Chen, Y. H., Keegan, S., Kahli, M., Tonzi, P., Fenyö, D., Huang, T. T., and Smith, D. J. (2019).
543 Transcription shapes DNA replication initiation and termination in human cells. Nat Struct
544 Mol Biol *26*, 67-77.

545 Ciccia, A., and Elledge, S. J. (2010). The DNA damage response: making it safe to play with
546 knives. Mol Cell *40*, 179-204.

547 Clausen, A. R., Lujan, S. A., Burkholder, A. B., Orebaugh, C. D., Williams, J. S., Clausen, M. F.,
548 Malc, E. P., Mieczkowski, P. A., Fargo, D. C., Smith, D. J., and Kunkel, T. A. (2015).
549 Tracking replication enzymology in vivo by genome-wide mapping of ribonucleotide
550 incorporation. Nat Struct Mol Biol *22*, 185-191.

551 Daigaku, Y., Keszthelyi, A., Muller, C. A., Miyabe, I., Brooks, T., Retkute, R., Hubank, M.,
552 Nieduszynski, C. A., and Carr, A. M. (2015). A global profile of replicative polymerase
553 usage. Nat Struct Mol Biol *22*, 192-198.

554 Devbhandari, S., Jiang, J., Kumar, C., Whitehouse, I., and Remus, D. (2017). Chromatin
555 Constrains the Initiation and Elongation of DNA Replication. Mol Cell *65*, 131-141.

556 Dicarlo, J. E., Norville, J. E., Mali, P., Rios, X., Aach, J., and Church, G. M. (2013). Genome
557 engineering in Saccharomyces cerevisiae using CRISPR-Cas systems. Nucleic Acids Res

558 Dubarry, M., Lawless, C., Banks, A. P., Cockell, S., and Lydall, D. (2015). Genetic Networks
559 Required to Coordinate Chromosome Replication by DNA Polymerases α, δ, and ε in
560 Saccharomyces cerevisiae. G3 (Bethesda) *5*, 2187-2197.

561 Evrin, C., Maman, J. D., Diamante, A., Pellegrini, L., and Labib, K. (2018). Histone H2A-H2B
562 binding by Pol α in the eukaryotic replisome contributes to the maintenance of repressive
563 chromatin. EMBO J *37*,

564 Foltman, M., Evrin, C., De Piccoli, G., Jones, R. C., Edmondson, R. D., Katou, Y., Nakato, R.,
565 Shirahige, K., and Labib, K. (2013). Eukaryotic replisome components cooperate to
566 process histones during chromosome replication. Cell Rep *3*, 892-904.

567 Fumasoni, M., Zwicky, K., Vanoli, F., Lopes, M., and Branzei, D. (2015). Error-Free DNA
568 Damage Tolerance and Sister Chromatid Proximity during DNA Replication Rely on the
569 Polalpha/Primase/Ctf4 Complex. Mol Cell *57*, 812-823.

570 Gambus, A., van Deursen, F., Polychronopoulos, D., Foltman, M., Jones, R. C., Edmondson, R.
571 D., Calzada, A., and Labib, K. (2009). A key role for Ctf4 in coupling the MCM2-7 helicase
572 to DNA polymerase alpha within the eukaryotic replisome. EMBO J *28*, 2992-3004.

573 Garbacz, M. A., Lujan, S. A., Burkholder, A. B., Cox, P. B., Wu, Q., Zhou, Z. X., Haber, J. E.,
574 and Kunkel, T. A. (2018). Evidence that DNA polymerase δ contributes to initiating leading
575 strand DNA replication in Saccharomyces cerevisiae. Nat Commun *9*, 858.

576 Glover, T. W., Berger, C., Coyle, J., and Echo, B. (1984). DNA polymerase alpha inhibition by
577 aphidicolin induces gaps and breaks at common fragile sites in human chromosomes.
578 Hum Genet *67*, 136-142.

579 Hamperl, S., Bocek, M. J., Saldivar, J. C., Swigut, T., and Cimprich, K. A. (2017). Transcription-
580 Replication Conflict Orientation Modulates R-Loop Levels and Activates Distinct DNA
581 Damage Responses. Cell *170*, 774-786.e19.

582 Hanna, J. S., Kroll, E. S., Lundblad, V., and Spencer, F. A. (2001). Saccharomyces cerevisiae
583 CTF18 and CTF4 are required for sister chromatid cohesion. Mol Cell Biol *21*, 3144-3158.

584 Haruki, H., Nishikawa, J., and Laemmli, U. K. (2008). The anchor-away technique: rapid,
585 conditional establishment of yeast mutant phenotypes. Mol Cell *31*, 925-932.

586 Ivessa, A. S., Lenzmeier, B. A., Bessler, J. B., Goudsouzian, L. K., Schnakenberg, S. L., and
587 Zakian, V. A. (2003). The Saccharomyces cerevisiae helicase Rrm3p facilitates replication
588 past nonhistone protein-DNA complexes. Mol Cell *12*, 1525-1536.

589 Jiang, C., and Pugh, B. F. (2009). A compiled and systematic reference map of nucleosome
590 positions across the Saccharomyces cerevisiae genome. Genome Biol *10*, R109.

591 Knott, S. R., Peace, J. M., Ostrow, A. Z., Gan, Y., Rex, A. E., Viggiani, C. J., Tavare, S., and
592 Aparicio, O. M. (2012). Forkhead Transcription Factors Establish Origin Timing and Long-
593 Range Clustering in S. cerevisiae. Cell *148*, 99-111.

594 Kouprina, N., Kroll, E., Bannikov, V., Bliskovsky, V., Gizatullin, R., Kirillov, A., Shestopalov, B.,
595 Zakharyev, V., Hieter, P., and Spencer, F. (1992). CTF4 (CHL15) mutants exhibit
596 defective DNA metabolism in the yeast Saccharomyces cerevisiae. Mol Cell Biol *12*, 5736-
597 5747.

598 Kunkel, T. A. (2011). Balancing eukaryotic replication asymmetry with replication fidelity. Curr
599 Opin Chem Biol *15*, 620-626.

600 Kunkel, T. A., and Burgers, P. M. (2008). Dividing the workload at a eukaryotic replication fork.
601 Trends Cell Biol *18*, 521-527.

602 Kurat, C. F., Yeeles, J. T., Patel, H., Early, A., and Diffley, J. F. (2017). Chromatin Controls DNA
603 Replication Origin Selection, Lagging-Strand Synthesis, and Replication Fork Rates. Mol
604 Cell *65*, 117-130.

605 Kwan, E. X., Wang, X. S., Amemiya, H. M., Brewer, B. J., and Raghuraman, M. K. (2016). rDNA
606 Copy Number Variants Are Frequent Passenger Mutations in Saccharomyces cerevisiae
607 Deletion Collections and de Novo Transformants. G3 (Bethesda) *6*, 2829-2838.

608 Lemoine, F. J., Degtyareva, N. P., Lobachev, K., and Petes, T. D. (2005). Chromosomal
609 translocations in yeast induced by low levels of DNA polymerase a model for chromosome
610 fragile sites. Cell *120*, 587-598.

611 McGuffee, S. R., Smith, D. J., and Whitehouse, I. (2013). Quantitative, Genome-Wide Analysis
612 of Eukaryotic Replication Initiation and Termination. Mol Cell *50*, 123-135.

613 Miyabe, I., Mizuno, K., Keszthelyi, A., Daigaku, Y., Skouteri, M., Mohebi, S., Kunkel, T. A.,
614 Murray, J. M., and Carr, A. M. (2015). Polymerase δ replicates both strands after
615 homologous recombination-dependent fork restart. Nat Struct Mol Biol *22*, 932-938.

616 Muzi Falconi, M., Piseri, A., Ferrari, M., Lucchini, G., Plevani, P., and Foiani, M. (1993). De novo
617 synthesis of budding yeast DNA polymerase alpha and POL1 transcription at the G1/S
618 boundary are not required for entrance into S phase. Proc Natl Acad Sci U S A *90*, 10519-
619 10523.

620 Ogawa, T., and Okazaki, T. (1980). Discontinuous DNA replication. Annu Rev Biochem *49*, 421-
621 457.

622 Osborn, A. J., and Elledge, S. J. (2003). Mrc1 is a replication fork component whose
623 phosphorylation in response to DNA replication stress activates Rad53. Genes Dev *17*,
624 1755-1767.

625 Osmundson, J. S., Kumar, J., Yeung, R., and Smith, D. J. (2017). Pif1-family helicases
626 cooperatively suppress widespread replication-fork arrest at tRNA genes. Nat Struct Mol
627 Biol *24*, 162-170.

628 Petryk, N., Kahli, M., d'Aubenton-Carafa, Y., Jaszczyszyn, Y., Shen, Y., Silvain, M., Thermes,
629 C., Chen, C. L., and Hyrien, O. (2016). Replication landscape of the human genome. Nat
630 Commun *7*, 10208.

631 Pourkarimi, E., Bellush, J. M., and Whitehouse, I. (2016). Spatiotemporal coupling and
632 decoupling of gene transcription with DNA replication origins during embryogenesis in C.
633 elegans. Elife *5*,

634 Pursell, Z. F., Isoz, I., Lundstrom, E. B., Johansson, E., and Kunkel, T. A. (2007). Yeast DNA
635 polymerase epsilon participates in leading-strand DNA replication. Science *317*, 127-130.

636 Reijns, M. A., Kemp, H., Ding, J., de Procé, S. M., Jackson, A. P., and Taylor, M. S. (2015).
637 Lagging-strand replication shapes the mutational landscape of the genome. Nature *518*,
638 502-506.

639 Samora, C., Saksouk, J., Goswami, P., Wade, B., Singleton, M., Bates, P., Lengronne, A.,
640 Costa, A., and Uhlmann, F. (2016). Ctf4 Links DNA Replication with Sister Chromatid
641 Cohesion Establishment by Recruiting the Chl1 Helicase to the Replisome. Molecular Cell
642 *63*, 371-384.

643 Sasaki, M., and Kobayashi, T. (2017). Ctf4 Prevents Genome Rearrangements by Suppressing
644 DNA Double-Strand Break Formation and Its End Resection at Arrested Replication Forks.
645 Molecular Cell *66*, 533-545.e5.

646 Shah, K. A., Shishkin, A. A., Voineagu, I., Pavlov, Y. I., Shcherbakova, P. V., and Mirkin, S. M.
647 (2012). Role of DNA polymerases in repeat-mediated genome instability. Cell Rep *2*,
648 1088-1095.

649 Shyian, M., Mattarocci, S., Albert, B., Hafner, L., Lezaja, A., Costanzo, M., Boone, C., and
650 Shore, D. (2016). Budding Yeast Rif1 Controls Genome Integrity by Inhibiting rDNA
651 Replication. PLoS Genet *12*, e1006414.

652 Simon, A. C., Zhou, J. C., Perera, R. L., van, D., Frederick, Evrin, C., Ivanova, M. E., Kilkenny,
653 M. L., Renault, L., Kjaer, S., Matak-Vinković, D., Labib, K., Costa, A., and Pellegrini, L.
654 (2014). A Ctf4 trimer couples the CMG helicase to DNA polymerase α in the eukaryotic
655 replisome. Nature *510*, 293-297.

656 Smith, D. J., and Whitehouse, I. (2012). Intrinsic coupling of lagging-strand synthesis to
657 chromatin assembly. Nature *483*, 434-438.

658 Song, W., Dominska, M., Greenwell, P. W., and Petes, T. D. (2014). Genome-wide high-
659 resolution mapping of chromosome fragile sites in Saccharomyces cerevisiae. Proc Natl
660 Acad Sci U S A *111*, E2210-8.

661 Szyjka, S. J., Viggiani, C. J., and Aparicio, O. M. (2005). Mrc1 is required for normal progression
662 of replication forks throughout chromatin in S. cerevisiae. Mol Cell *19*, 691-697.

663 Tanaka, H., Katou, Y., Yagura, M., Saitoh, K., Itoh, T., Araki, H., Bando, M., and Shirahige, K.
664 (2009). Ctf4 coordinates the progression of helicase and DNA polymerase alpha. Genes
665 Cells *14*, 807-820.

666 Taylor, M. R. G., and Yeeles, J. T. P. (2018). The Initial Response of a Eukaryotic Replisome to
667 DNA Damage. Molecular Cell *70*, 1067-1080.

668 Tran, P. L. T., Pohl, T. J., Chen, C. F., Chan, A., Pott, S., and Zakian, V. A. (2017). PIF1 family
669 DNA helicases suppress R-loop mediated genome instability at tRNA genes. Nat Commun
670 *8*, 15025.

671 Van Esch, H., Colnaghi, R., Freson, K., Starokadomskyy, P., Zankl, A., Backx, L., Abramowicz,
672 I., Outwin, E., Rohena, L., Faulkner, C., Leong, G. M., Newbury-Ecob, R. A., Challis, R. C.,
673 Õunap, K., Jaeken, J., Seuntjens, E., Devriendt, K., Burstein, E., Low, K. J., and
674 O'Driscoll, M. (2019). Defective DNA Polymerase α-Primase Leads to X-Linked Intellectual
675 Disability Associated with Severe Growth Retardation, Microcephaly, and Hypogonadism.
676 Am J Hum Genet *104*, 957-967.

677 Villa, F., Simon, A. C., Ortiz Bazan, M. A., Kilkenny, M. L., Wirthensohn, D., Wightman, M.,
678 Matak-Vinkovíc, D., Pellegrini, L., and Labib, K. (2016). Ctf4 Is a Hub in the Eukaryotic
679 Replisome that Links Multiple CIP-Box Proteins to the CMG Helicase. Mol Cell *63*, 385-
680 396.

681 Wu, C. A., Zechner, E. L., Reems, J. A., McHenry, C. S., and Marians, K. J. (1992). Coordinated
682 leading- and lagging-strand synthesis at the Escherichia coli DNA replication fork. V.
683 Primase action regulates the cycle of Okazaki fragment synthesis. J Biol Chem *267*, 4074-
684 4083.

685 Yadav, T., and Whitehouse, I. (2016). Replication-Coupled Nucleosome Assembly and
686 Positioning by ATP-Dependent Chromatin-Remodeling Enzymes. Cell Rep

687 Yeeles, J. T., Janska, A., Early, A., and Diffley, J. F. (2017). How the Eukaryotic Replisome
688 Achieves Rapid and Efficient DNA Replication. Mol Cell *65*, 105-116.

689 Yoshida, K., Bacal, J., Desmarais, D., Padioleau, I., Tsaponina, O., Chabes, A., Pantesco, V.,
690 Dubois, E., Parrinello, H., Skrzypczak, M., Ginalski, K., Lengronne, A., and Pasero, P.
691 (2014). The histone deacetylases sir2 and rpd3 act on ribosomal DNA to control the
692 replication program in budding yeast. Mol Cell *54*, 691-697.

693 Zhu, W., Ukomadu, C., Jha, S., Senga, T., Dhar, S. K., Wohlschlegel, J. A., Nutt, L. K.,
694 Kornbluth, S., and Dutta, A. (2007). Mcm10 and And-1/CTF4 recruit DNA polymerase
695 alpha to chromatin for initiation of DNA replication. Genes Dev *21*, 2288-2299.

696

697

698 **LEGENDS TO FIGURES**

699 **Figure 1. Okazaki fragments increase in length when Pol α is limiting.**

700 **(A).** Western blot against 13xMyc-tagged Pol1 from S. cerevisiae from a wild-type or *GDPOL1*
701 strain, as indicated, shifted to YPD or YEP + 3% raffinose (hereafter, media) supplemented with
702 various concentrations of galactose. The lower band indicated by an asterisk is a degradation
703 product resulting from degron-tagging.

704 **(B).** Schematic of experimental workflow for Okazaki fragment analysis and sequencing (also
705 see methods).

706 **(C, D).** Alkaline agarose gel analysis of end-labeled Okazaki fragments from a wild type (C) or
707 *GDPOL1* (D) strain, shifted to YPD or media supplemented with galactose as indicated.

708 **(E).** Southern blot using a whole genome probe, on Okazaki fragments from a wild type or
709 *GDPOL1* strain shifted to media with the indicated sugar concentrations.

710 **(F, G).** Distribution of Okazaki fragment 5' ends around consensus nucleosome dyads (Jiang
711 and Pugh, 2009) for a wild-type (F) or *GDPOL1* (G) strain shifted to media containing the
712 indicated concentration of galactose. Data for Okazaki fragment 3' ends in *GDPOL1* are in Fig.
713 S1F

714

715 **Figure 2. Origin firing efficiency is decreased for all replication origins when Pol α levels**
716 **are reduced**

717 **(A).** Okazaki fragment distributions from a wild-type (black) or *GDPOL1* strain shifted to the
718 indicated media. A ~200 kb region from the right arm of chromosome 10 is shown, and three
719 efficient origins are annotated.

720 **(B).** Origin efficiency calculated as OEM (see methods) in wild-type or *GDPOL1* cells shifted to
721 the indicated concentration of galactose. Data is in the form of box and whisker plots with the
722 ends of the boxes being the upper and lower quartiles, the median is denoted by the line within

723 the box, and the whiskers indicate the highest and lowest data points. Origin efficiency was
724 calculated as in (McGuffee et al., 2013), using origin locations annotated in the same study.
725 Significance was calculated by unpaired t-test; **** $p<0.0001$, * $p<0.05$. Data from the *GDPOL1*
726 strain are the average of three replicates.
727 **(C).** Scatter plot comparing origin firing efficiency in *GDPOL1* cells at 0.014% galactose, to wild-
728 type cells in 0.5% galactose. Analogous comparisons to other galactose concentrations, and
729 correlations between replicates, are in Fig. S2.
730 **(D).** Scatter plot showing the percentage decrease in origin firing efficiency, relative to wild-type
731 cells, for *GDPOL1* cells shifted to the indicated galactose concentrations. Origins were ordered
732 by their firing efficiency in wild-type cells at 0.5% galactose. Each origin efficiency spot
733 represents the average of three replicates.
734 **(E).** Firing efficiency for origins with replication timing below (early) or above (late) the median
735 replication timing for origins in our dataset.
736
737 **Figure 3. Ctf4 maintains Okazaki fragment length at low Pol α concentrations but is**
738 **dispensable for origin firing in vivo**
739 **(A, B, C).** Alkaline agarose gel analysis of end-labeled Okazaki fragments from a wild type or
740 *GDPOL1;ctf4Δ* strain (A&B), or *GDpol1-4A* (C) as indicated, shifted to media containing various
741 concentrations of galactose. Note that the range of galactose concentrations in A is significantly
742 higher than in other figure panels. Traces of lanes are shown for wild type YPD (black), or
743 *GDPOL1* 0.5% (gray) and 0.05% galactose (blue).
744 **(D, E).** Replication origin efficiency, as in Fig. 2B, for *GDPOL1;ctf4Δ* (D) or *GDpol1-4A* (E) cells
745 at low galactose concentrations. Data were calculated and analyzed as in Fig. 2B.

746 **(F).** Distribution of Okazaki fragment 5' termini around consensus nucleosome dyads, as in Fig.
747 1F,G, for each indicated strain shifted to media containing 0.05% galactose. Data were
748 calculated and analyzed as in Fig. 1F&G.
749
750 **Figure 4. The checkpoint is required for viability under conditions of limiting origin firing,**
751 **but not increased Okazaki fragment size.**
752 **(A).** Western blot against Rad53 from asynchronous *GDPOL1* cells shifted to the indicated
753 media. A wild-type strain grown in YPGal ± 0.1% MMS were used as negative and positive
754 controls for Rad53 hyperphosphorylation.
755 **(B).** Serial dilution spot tests to assay the growth of *GDPOL1* strains carrying additional
756 mutations (*mec1Δ;sml1Δ, rad9Δ, mrc1Δ, rad9Δ;mrc1Δ;sml1Δ*) at the indicated galactose
757 concentrations.
758 **(C).** Southern blot as in Fig. 3B, for a *mec1Δ;GDPOL1* strain shifted to various galactose
759 concentrations.
760 **(D).** Serial dilution spot tests to assay the growth of *GDPOL1* strains carrying additional
761 mutations (*rad9Δ, mrc1*^{AQ,} *rad9Δ;mrc1*^{AQ}) at the indicated galactose concentrations.
762 **(E).** Serial dilution spot tests to assay the growth of *ctf4Δ;GDPOL1* or *GDpol1-4A* strains with or
763 without additional deletion of *MEC1*.
764
765 **Figure 5. Model of Pol α recruitment for leading- and lagging-strand priming in *S.***
766 ***cerevisiae***
767
768

Porcella et al., Figure 1

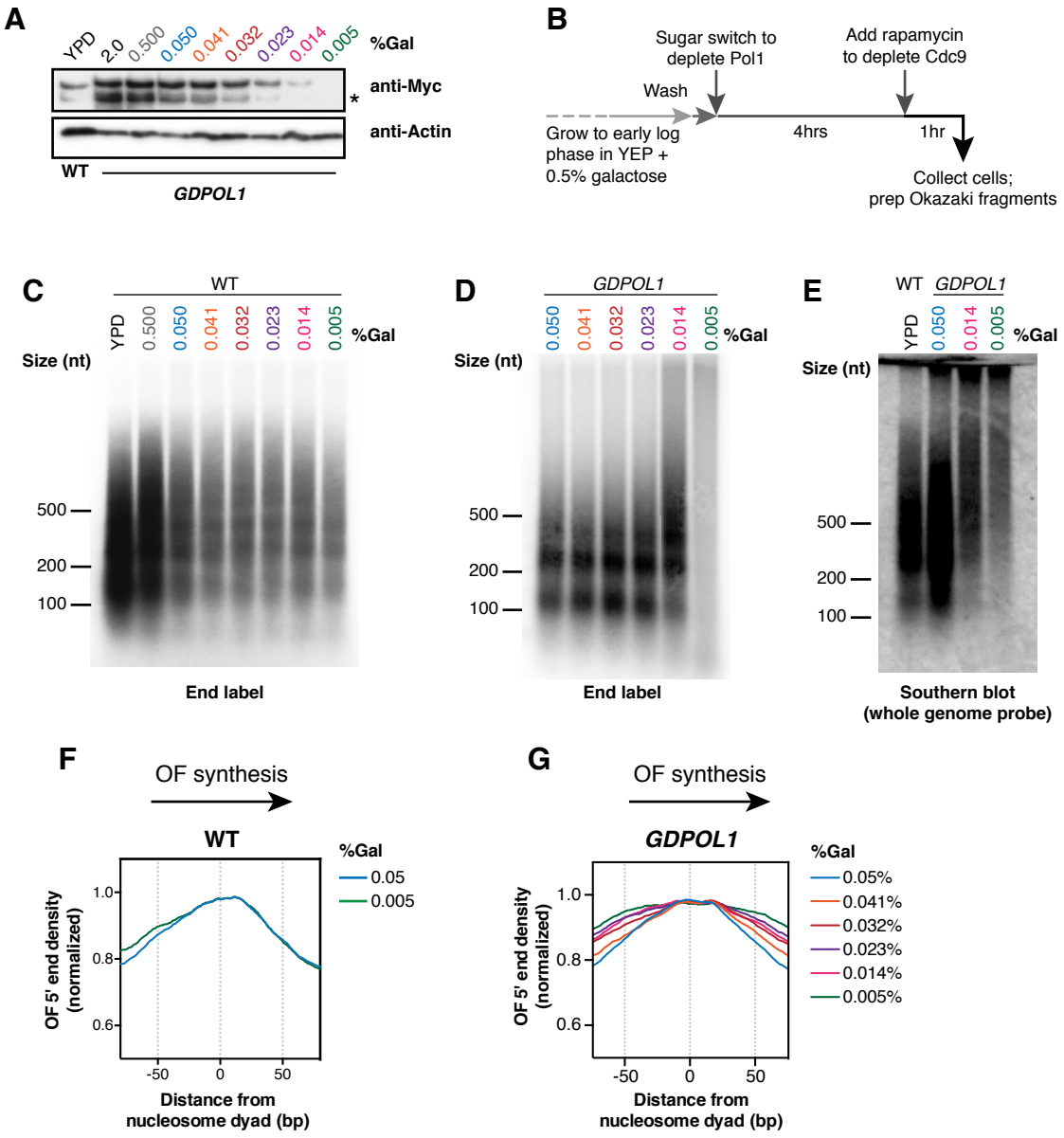

Porcella et al., Figure 2

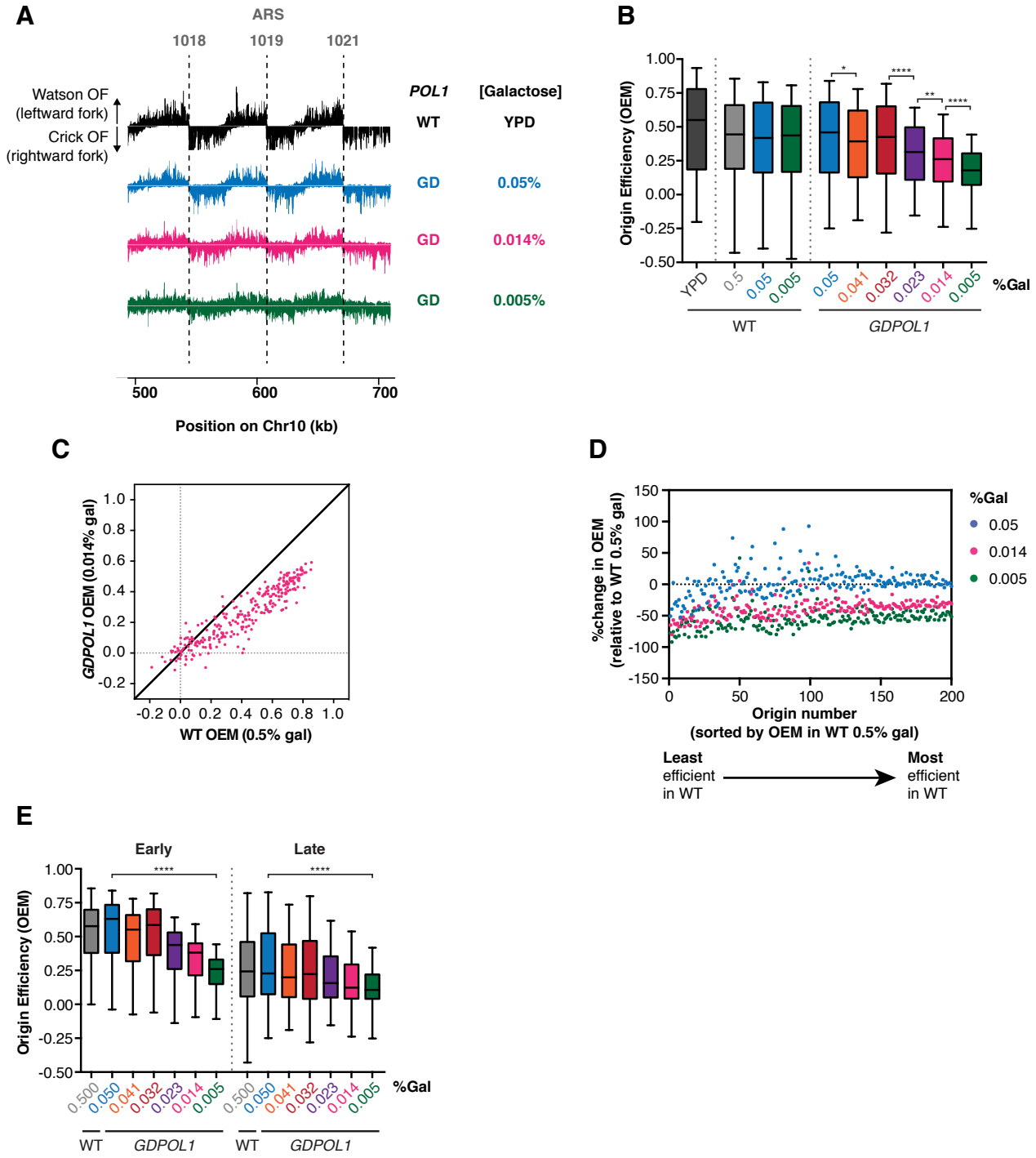

Porcella et al., Figure 3

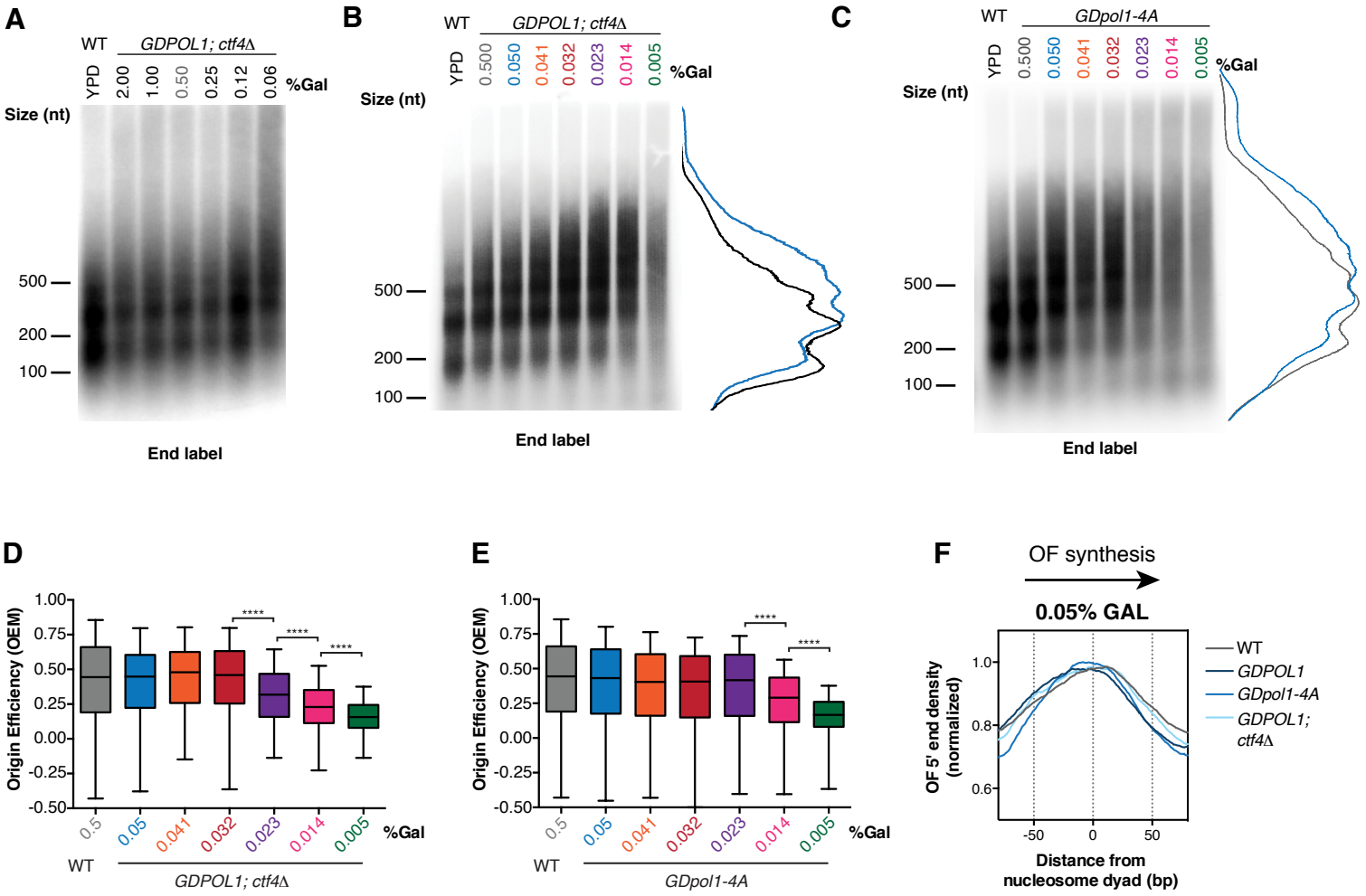

Porcella et al., Figure 4

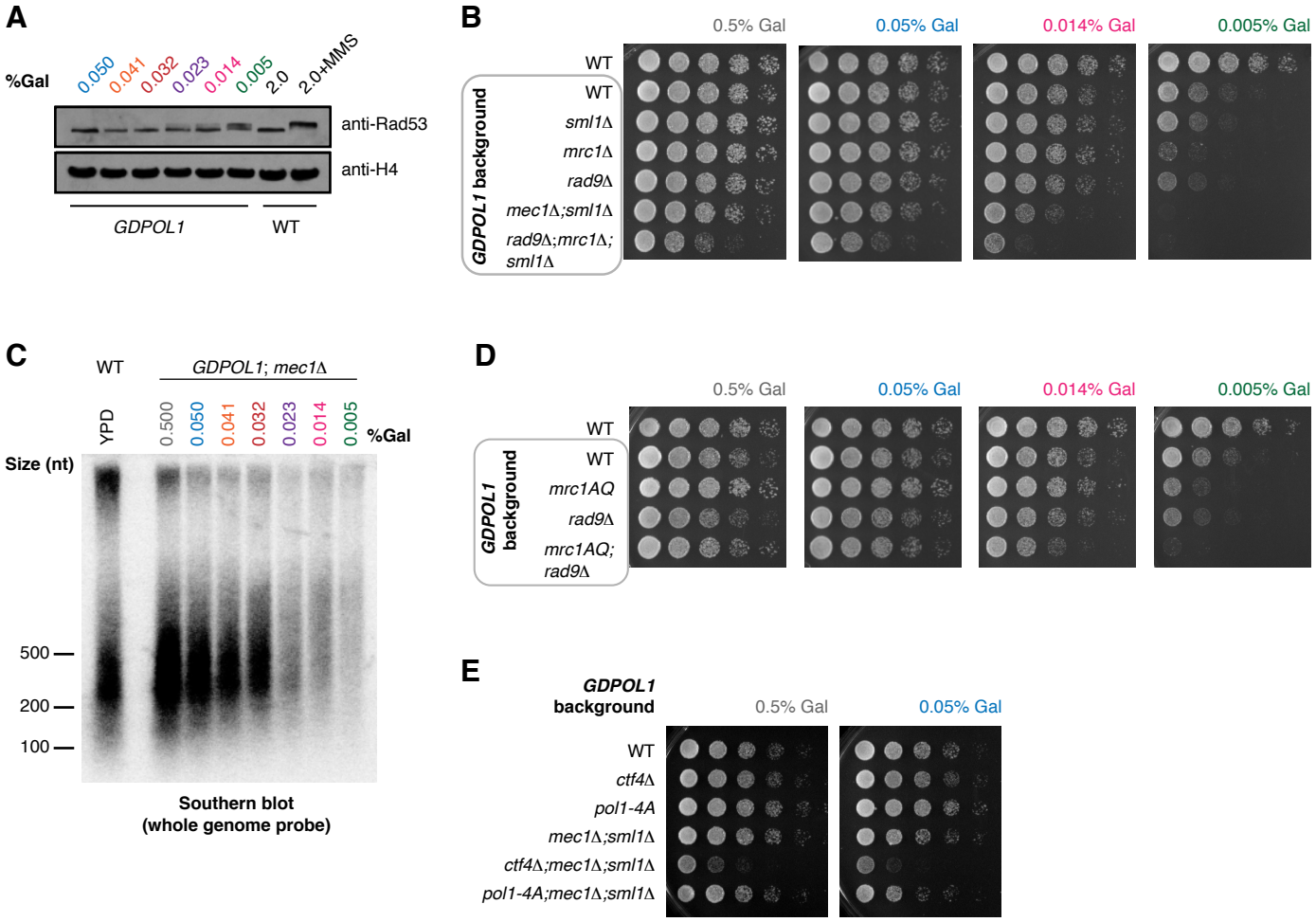

Porcella et al., Figure 5

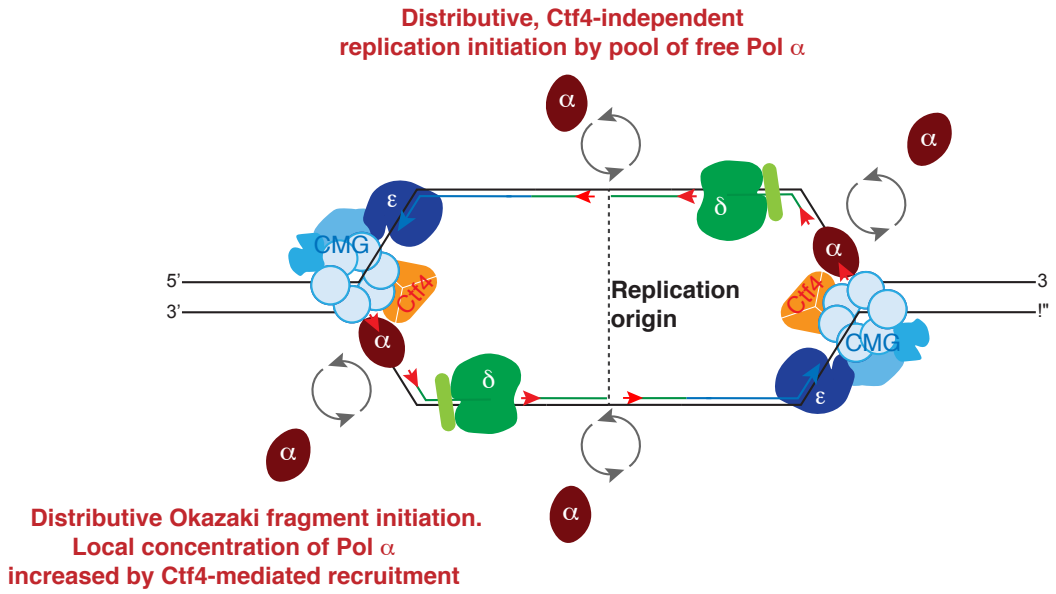

769 **LEGENDS TO SUPPLEMENTARY FIGURES**

770 **Figure S1 (Associated with Fig 1)**

771 **(A).** Western blot against 13xMyc-tagged Pol1 from wild-type or *GDPOL1* cells at the indicated
772 sugar concentration, released from alpha-factor arrest for the indicated time. The GDPol1-
773 specific degradation product is indicated by an asterisk.

774 **(B).** Timecourse of Okazaki fragment enrichment during Cdc9 nuclear depletion by anchor away
775 (Haruki et al., 2008). Okazaki fragments were prepared and labeled as in Fig. 1C, and as
776 previously described (Smith and Whitehouse, 2012).

777 **(C-E).** Representative replicate Okazaki fragment end-labeling gels for wild-type (C) and
778 *GDPOL1* (D-E) at the indicated galactose concentrations. Traces adjacent to the plots in D&E
779 indicate the change in size distribution of Okazaki fragments at 0.014% (pink) and 0.005%
780 (green) galactose.

781 **(F).** Distribution of Okazaki fragment 3' ends around consensus nucleosome dyads (Jiang and
782 Pugh, 2009) in the *GDPOL1* strain shifted to media containing the indicated concentration of
783 galactose

784

785 **Figure S2 (Associated with Fig 2)**

786 **(A).** Origin efficiency replicate comparisons for data from the *GDPOL1* strain shown in Fig. 2B
787 each of three replicates are plotted against each other and indicated by color.

788 **(B).** Comparison of origin efficiency data from each replicate from *GDPOL1* cells shifted to the
789 indicated concentration of galactose. Significance was calculated by unpaired t-test; ****
790 $p<0.0001$, * $p<0.05$.

791 **(C).** Scatter plots comparing origin firing efficiency in *GDPOL1* cells at various galactose
792 concentrations, to wild-type cells in 0.5% galactose.

793

794 **Figure S3 (Associated with Fig 2)**

795 **(A).** Doubling times for wild-type or *GDPOL1* strains in YEP + 3% raffinose, supplemented with
796 the indicated concentration of galactose. Data are the average of at least three replicates in
797 each case.

798 **(B).** DNA content, assayed by flow cytometry, of an arrest release of wild type or *GDPOL1* cells
799 also analyzed in A.

800 **(C).** DNA content, assayed by flow cytometry, of asynchronous cells post 4h sugar switch of
801 wild type or *GDPOL1* cells.

802

803 **Figure S4**

804 Analysis of replication-fork direction around 93 origin-distal tRNA genes (Osmundson et al.,
805 2017) in *GDPOL1* cells grown at various galactose concentrations. Increased replication-fork
806 stalling or arrest at these sites would manifest as a decrease at or after the midpoint of the gene
807 (Osmundson et al., 2017).

808

809 **Figure S5 (Associated with Fig 3)**

810 **(A-C).** Representative replicate end-labeling gel (A, C) or Southern blot (B), on Okazaki
811 fragments from a *GDPOL1;ctf4Δ* (A, B) or *GDpol1-4A* (C) strain shifted to media shifted to low
812 galactose concentrations. Traces of YPD (black) and 0.05% galactose (blue) lanes on the right.
813 A control lane for wild-type cells grown in YPD is included on each gel.

814 **(D).** Serial dilution spot tests to assay the growth of *GDPOL1* strains with or without FRB
815 tagging of CDC9 and/or *ctf4Δ* or *pol1-4A* mutations.

816 **(E).** The rDNA repeat is expanded in *ctf4Δ; GDPOL1* cells. The proportion of sequencing reads
817 mapping to the rDNA is indicated. Data represent the mean ± SD of all sequencing datasets
818 used for analysis in figures 2&3.

819 **(F-G).** Distribution of Okazaki fragment 5' (left panel) and 3' ends (right panel) around

820 consensus nucleosome dyads (Jiang and Pugh, 2009) in the *GDPOL1;ctf4Δ* (F) or *GDpol1-4A*

821 strain (G) shifted to media containing various galactose concentrations.

822 **Figure S6 (Associated with Fig 3)**

823 **(A, B).** Origin efficiency replicate comparisons for data from the *ctf4Δ;GDPOL1* strain shown in

824 Fig. 3D (A) and the *GDpol1-4A* strain show in Fig. 3F (B).

825

826 **Figure S7 (Associated with Fig 4)**

827 **(A, B).** Serial dilution spot tests to assay the growth of *GDPOL1* strains carrying additional

828 mutations (*mec1Δ;sml1Δ, rad9Δ, mrc1Δ, mrc1AQ*) at the indicated galactose concentrations. A

829 selection of these concentrations is shown in Fig. 4A-B

830 **(C,D).** Serial dilution spot tests of the indicated strains with or without 1 mM hydroxyurea (C) or

831 with or without 0.008% methyl methanesulfonate (D). Note that the full ranges of galactose

832 concentrations were independently plated as loading/growth controls for both C and D.

Porcella et al., Figure S1, associated with Figure 1

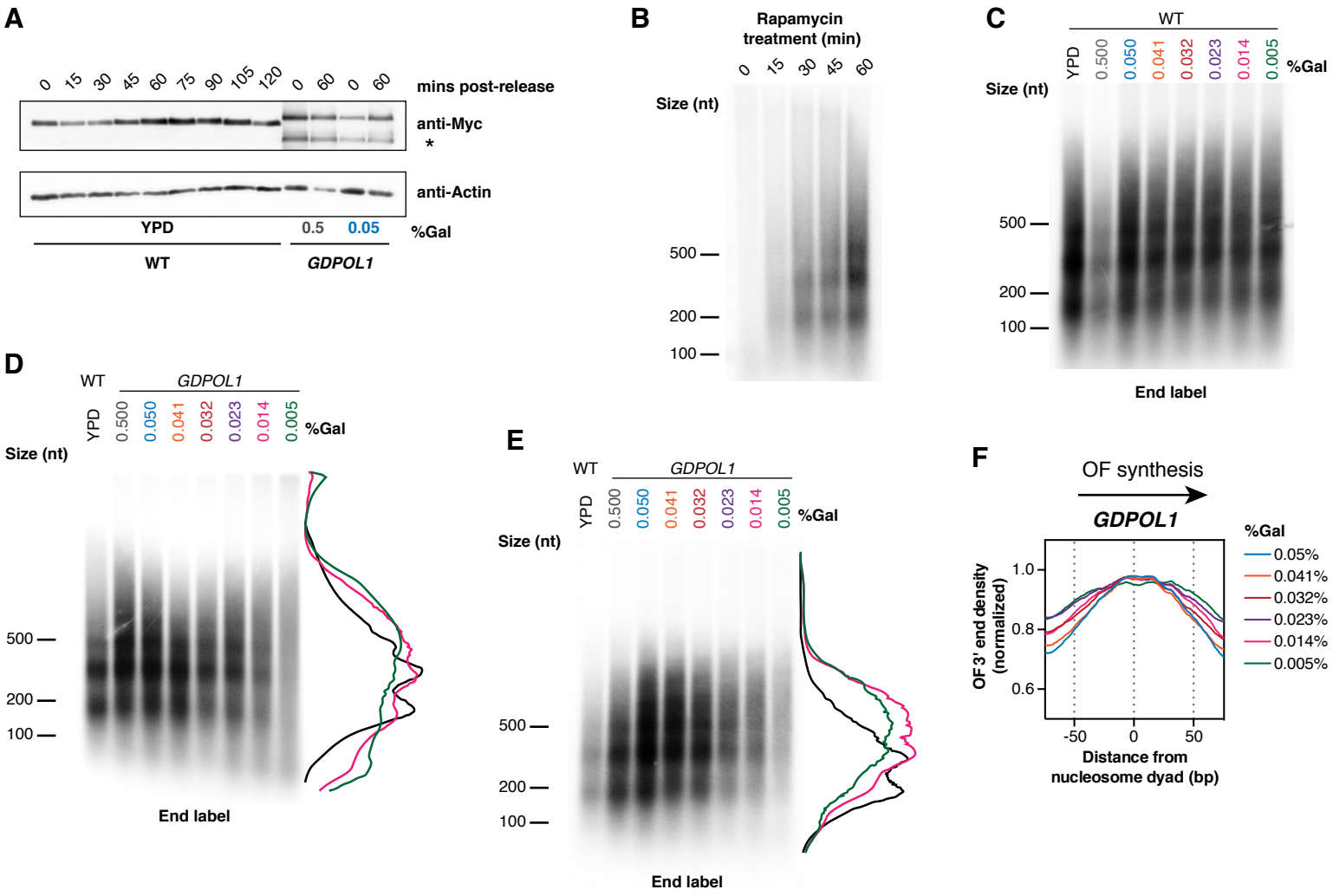

Porcella et al., Figure S2, associated with Figure 2

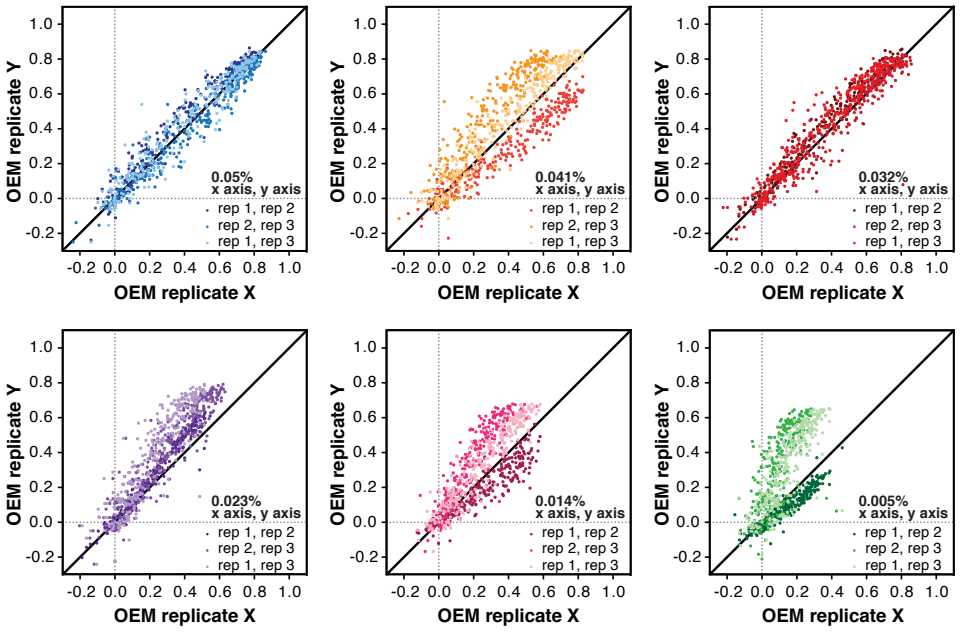

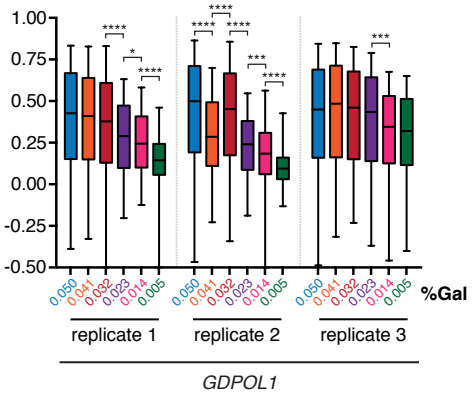

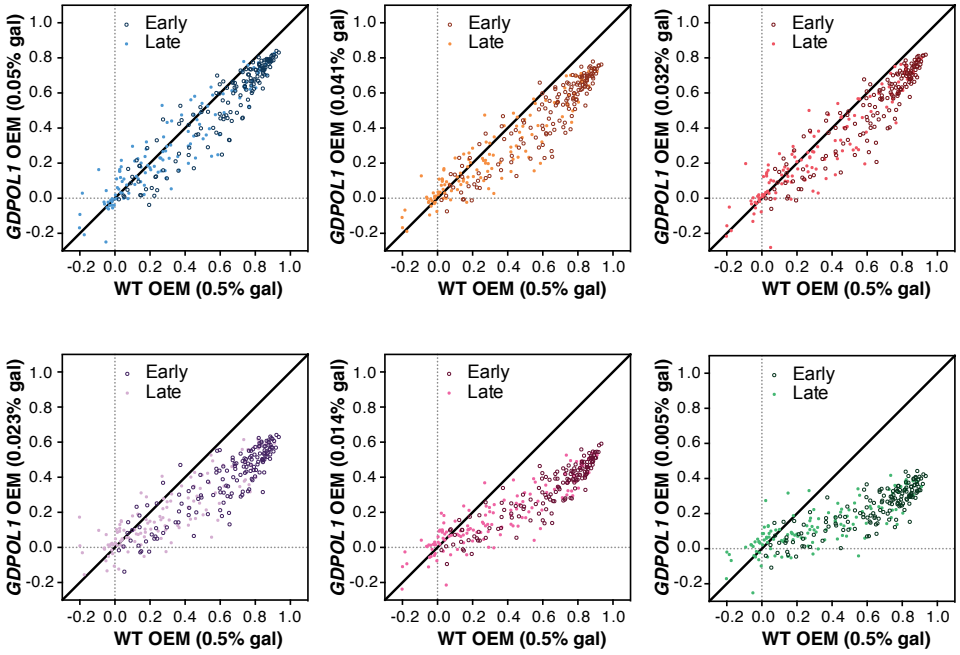

Porcella et al., Figure S3, associated with Figure 1

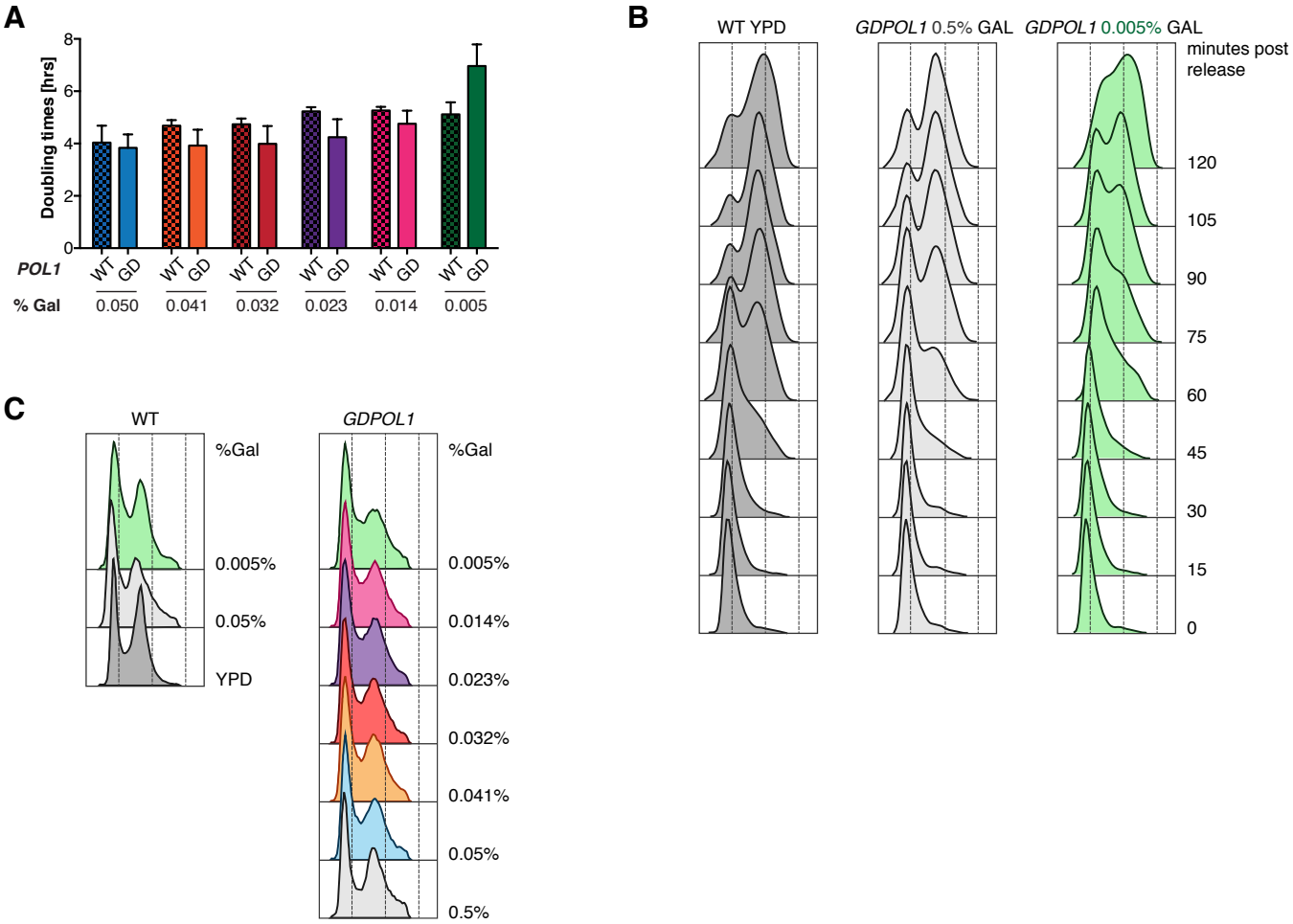

Porcella et al., Figure S4, associated with Figure 2

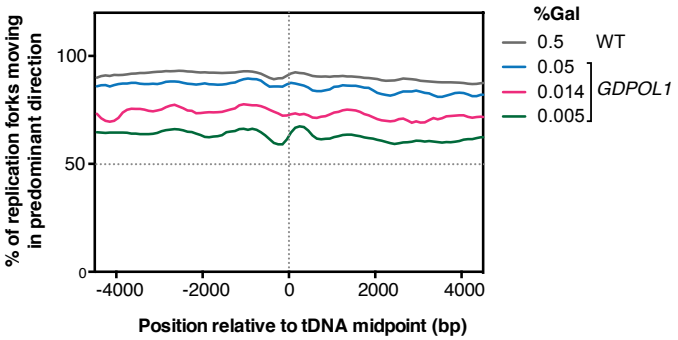

Porcella et al., Figure S5, associated with Figure 3

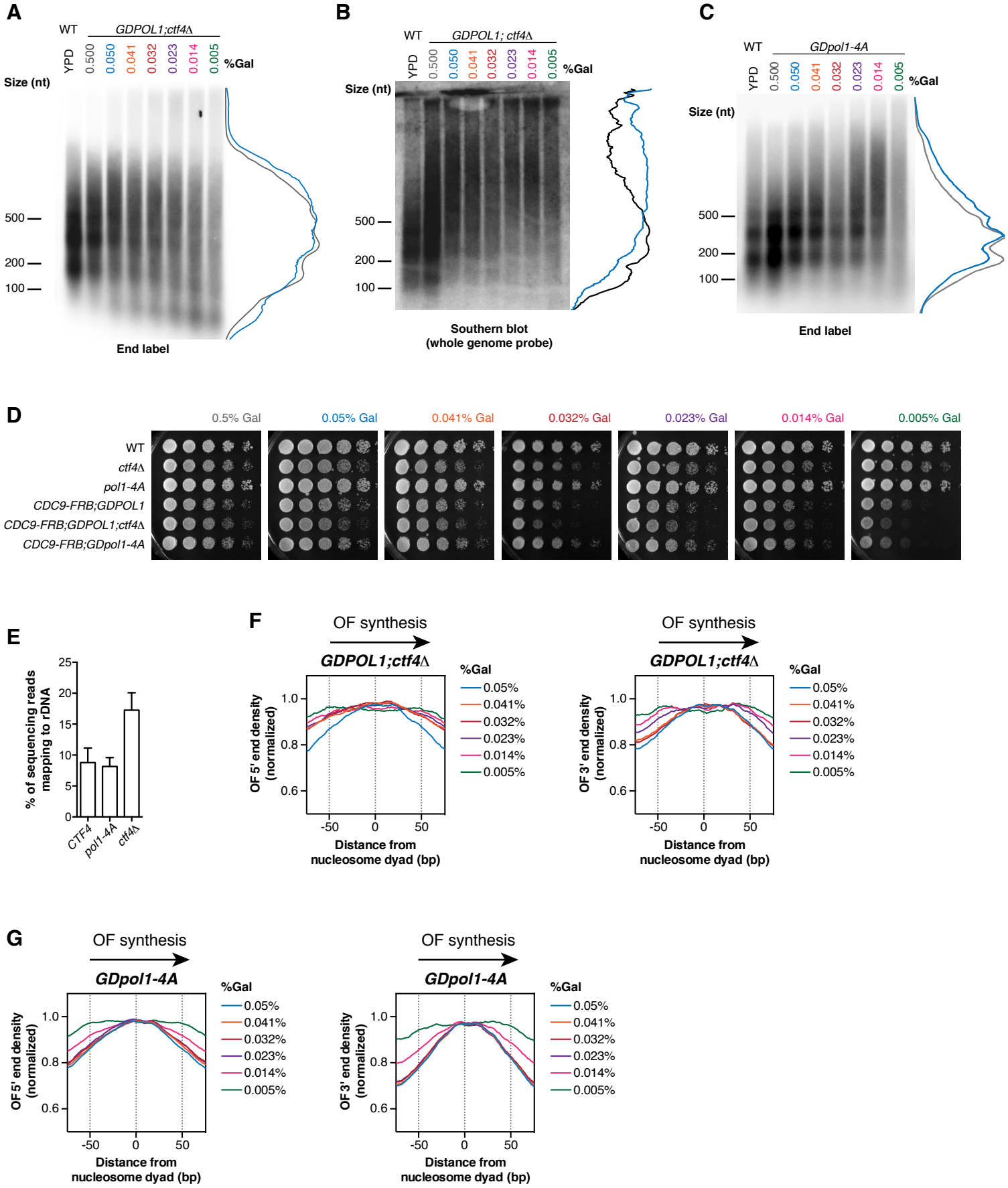

Porcella et al., Figure S6, associated with Figure 3

A **OEM correlations across replicates (*GDPOL1*, *ctf4*Δ)**

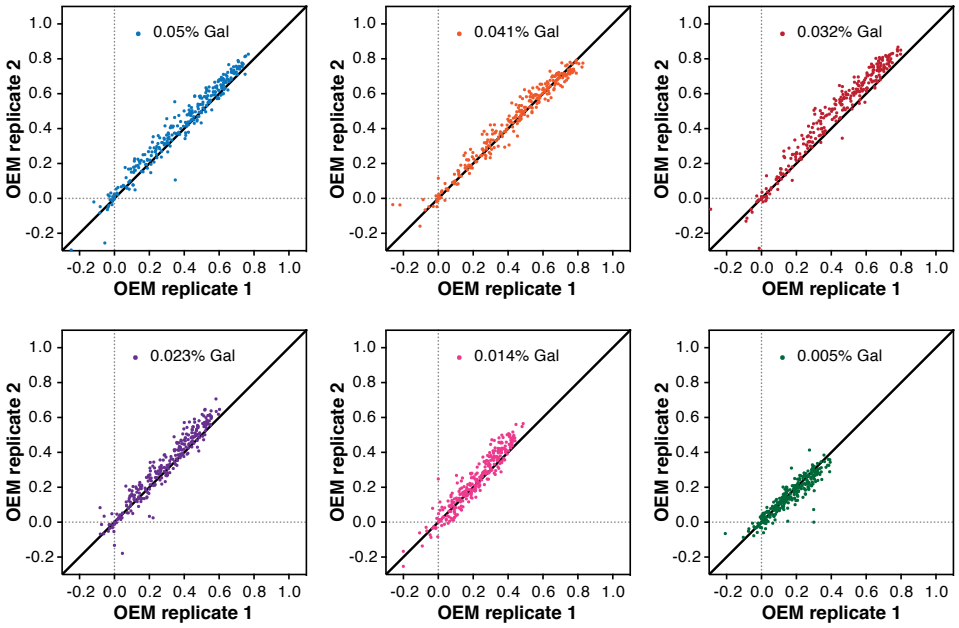

B **OEM correlations across replicates (*GDpol1-4A*)**

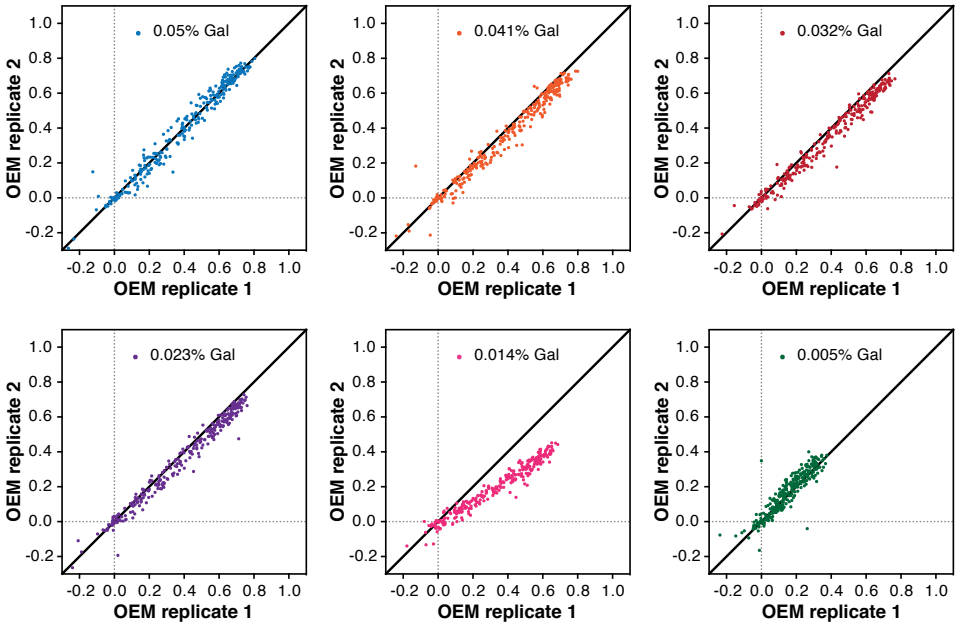
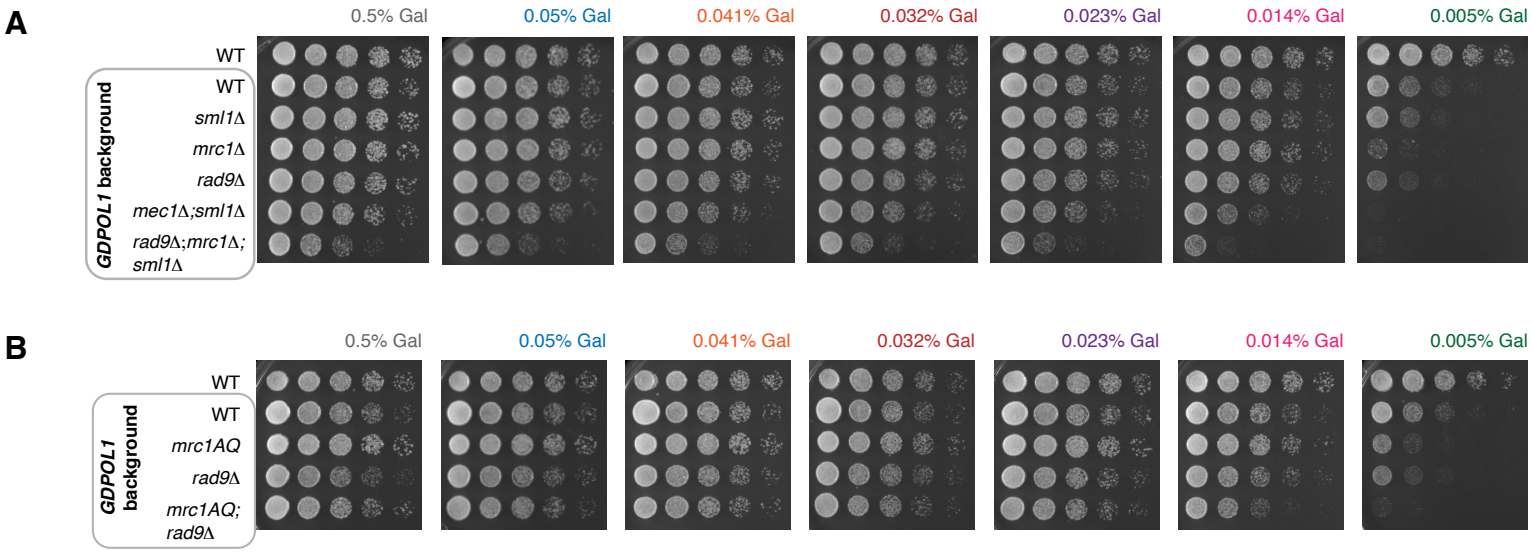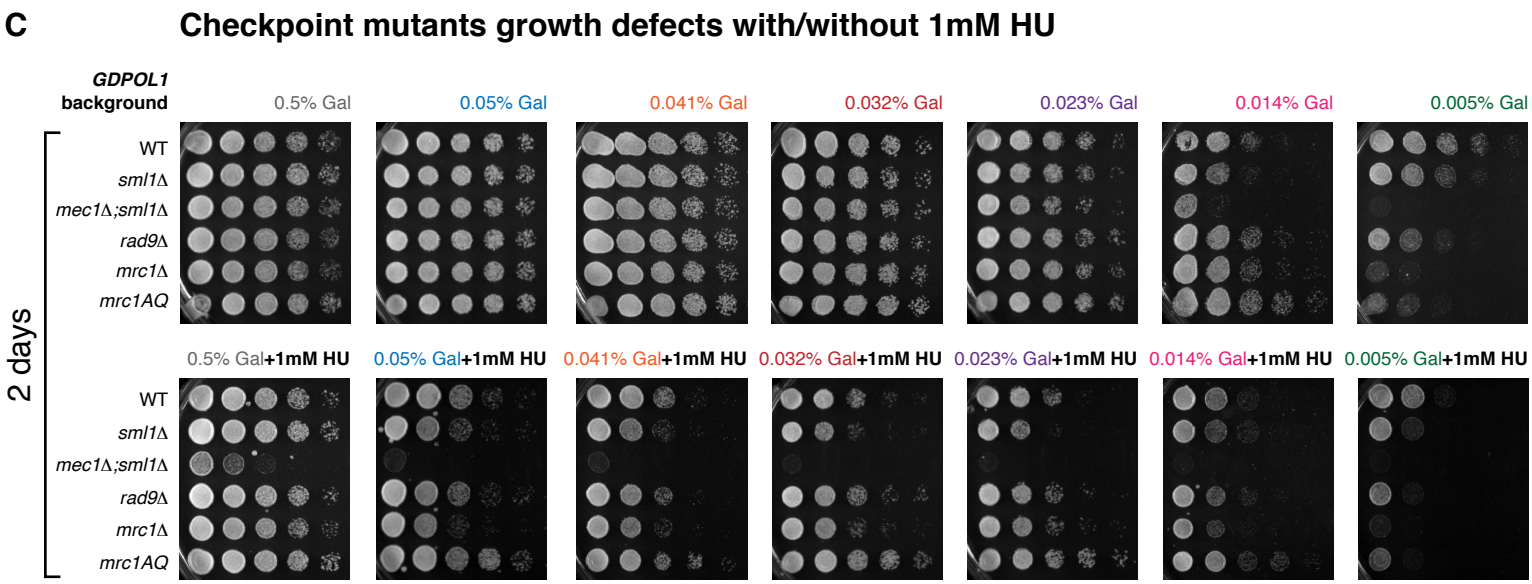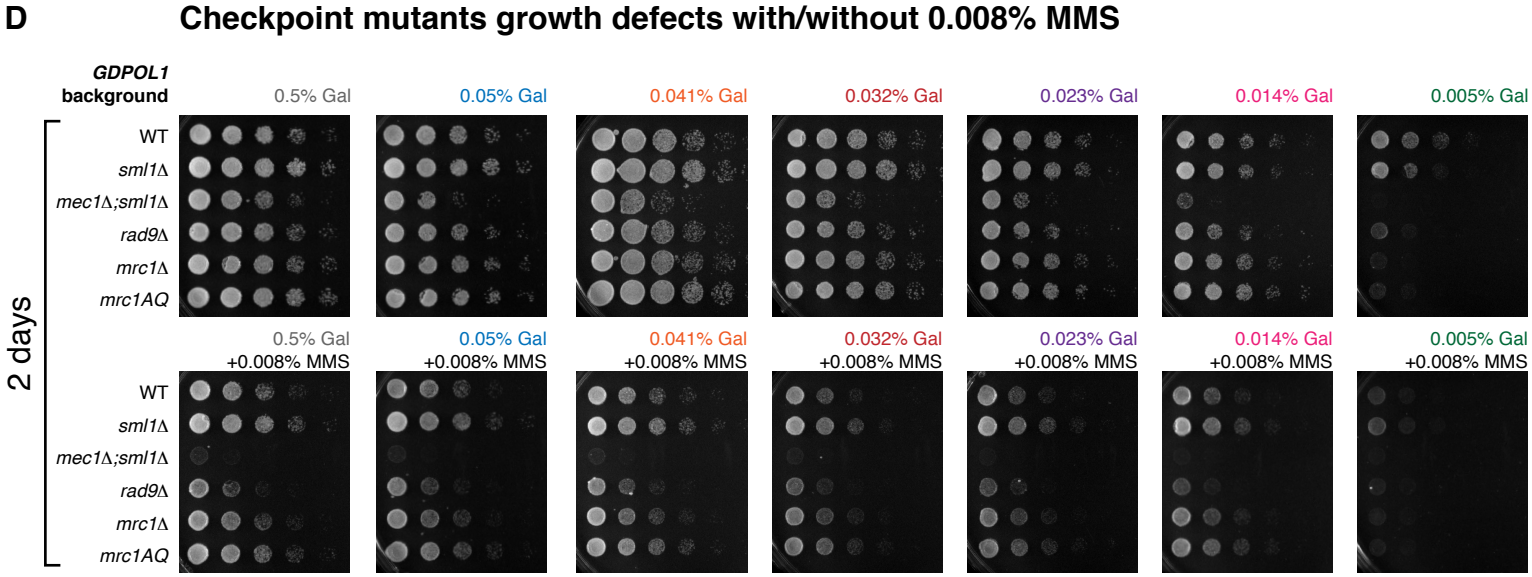
Porcella et al., Figure S7, associated with Figure 4